



Phox2a Defines a Developmental Origin of the Anterolateral System in Mice and Humans

R Brian Roome, Farin B Bourojeni, Bishakha Mona, Shima Rastegar-Pouyani, Raphael Blain, Annie Dumouchel, Charleen Salesse, W Scott Thompson, Megan Brookbank, Yorick Gitton, et al.

► To cite this version:

R Brian Roome, Farin B Bourojeni, Bishakha Mona, Shima Rastegar-Pouyani, Raphael Blain, et al.. Phox2a Defines a Developmental Origin of the Anterolateral System in Mice and Humans. Cell Reports, 2020, 33 (8), pp.108425. 10.1016/j.celrep.2020.108425 . hal-03087358

HAL Id: hal-03087358

<https://hal.science/hal-03087358>

Submitted on 23 Dec 2020

HAL is a multi-disciplinary open access archive for the deposit and dissemination of scientific research documents, whether they are published or not. The documents may come from teaching and research institutions in France or abroad, or from public or private research centers.

L'archive ouverte pluridisciplinaire **HAL**, est destinée au dépôt et à la diffusion de documents scientifiques de niveau recherche, publiés ou non, émanant des établissements d'enseignement et de recherche français ou étrangers, des laboratoires publics ou privés.



Published in final edited form as:

Cell Rep. 2020 November 24; 33(8): 108425. doi:10.1016/j.celrep.2020.108425.

Phox2a Defines a Developmental Origin of the Anterolateral System in Mice and Humans

R. Brian Roome^{1,2}, Farin B. Bourojeni^{1,2}, Bishakha Mona³, Shima Rastegar-Pouyani^{1,2}, Raphael Blain⁴, Annie Dumouchel¹, Charleen Salesse¹, W. Scott Thompson¹, Megan Brookbank¹, Yorick Gitton⁴, Lino Tessarollo⁵, Martyn Goulding⁶, Jane E. Johnson^{3,7}, Marie Kmita^{1,9}, Alain Chédotal⁴, Artur Kania^{1,2,8,9,10,*}

¹Institut de Recherches Cliniques de Montréal (IRCM), Montréal, QC H2W 1R7, Canada

²Integrated Program in Neuroscience, McGill University, Montréal, QC H3A 2B4, Canada

³Department of Neuroscience, University of Texas Southwestern Medical Center, Dallas, TX 75390, USA

⁴Sorbonne Université, INSERM, CNRS, Institut de la Vision, Paris 75012, France

⁵Neural Development Section, Mouse Cancer Genetics Program, National Cancer Institute, Frederick, MD 21702, USA

⁶Molecular Neurobiology Laboratory, The Salk Institute for Biological Studies, La Jolla, CA 92037, USA

⁷Department of Pharmacology, University of Texas Southwestern Medical Center, Dallas, TX 75390, USA

⁸Department of Anatomy and Cell Biology, McGill University, Montréal, QC H3A 0C7, Canada

⁹Division of Experimental Medicine, McGill University, Montréal, QC H3A 2B2, Canada

¹⁰Lead Contact

SUMMARY

Anterolateral system neurons relay pain, itch, and temperature information from the spinal cord to pain-related brain regions, but the differentiation of these neurons and their specific contribution to pain perception remain poorly defined. Here, we show that most mouse spinal neurons that embryonically express the autonomic-system-associated Paired-like homeobox 2A (Phox2a) transcription factor innervate nociceptive brain targets, including the parabrachial nucleus and the

*Correspondence: artur.kania@ircm.qc.ca.

AUTHOR CONTRIBUTIONS

Conceptualization, R.B.R. and A.K.; Methodology, R.B.R., B.M., R.B., C.S., J.E.J., A.D., and M.K.; Validation, R.B.R.; Formal Analysis, R.B.R. and B.M.; Investigation, R.B.R., F.B.B., B.M., S.R.-P., R.B., C.S., W.S.T., and M.B.; Resources, R.B.R., A.D., M.K., L.T., Y.G., M.G., and A.K.; Data Curation, R.B.R., B.M., and J.E.J.; Writing – Original Draft, R.B.R.; Writing – Review & Editing, R.B.R., F.B.B., S.R.-P., M.K., L.T., J.E.J., M.K., A.C., and A.K.; Visualization, R.B.R., B.M., and J.E.J.; Supervision, J.E.J., M.K., A.C., and A.K.; Project Administration, A.K.; Funding Acquisition, J.E.J., M.K., A.C., and A.K.

SUPPLEMENTAL INFORMATION

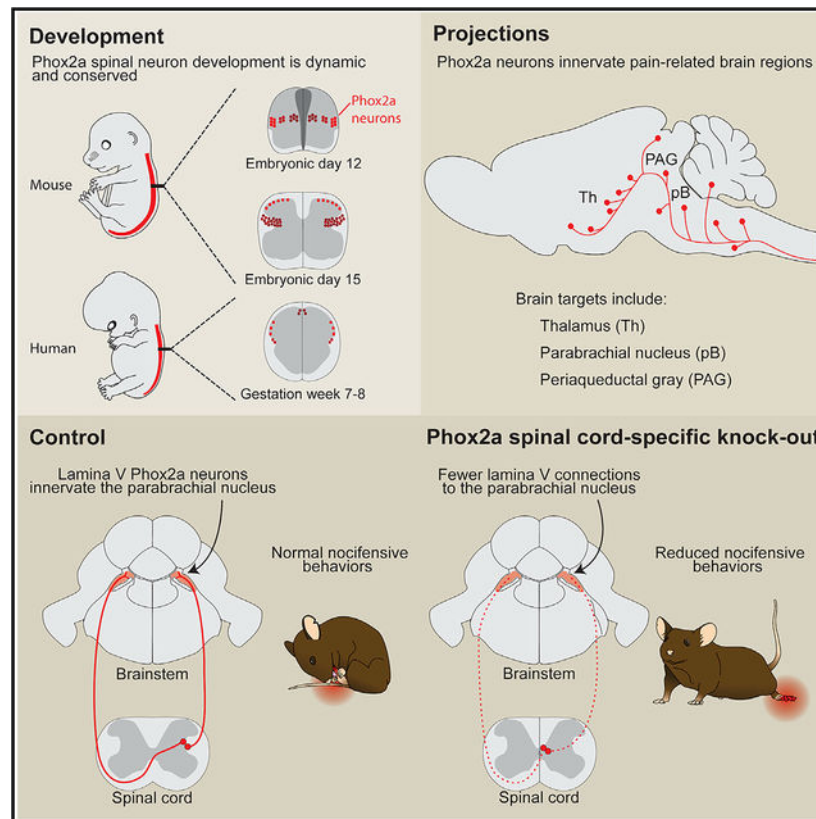
Supplemental Information can be found online at <https://doi.org/10.1016/j.celrep.2020.108425>.

DECLARATION OF INTERESTS

The authors declare no competing interests.

thalamus. We define the Phox2a anterolateral system neuron birth order, migration, and differentiation and uncover an essential role for Phox2a in the development of relay of nociceptive signals from the spinal cord to the brain. Finally, we also demonstrate that the molecular identity of Phox2a neurons is conserved in the human fetal spinal cord, arguing that the developmental expression of Phox2a is a prominent feature of anterolateral system neurons.

Graphical Abstract



In Brief

Roome et al. generate a Phox2a^{Cre} mouse that labels anterolateral system neurons during development, revealing their developmental dynamics as well as their molecular conservation in humans. Developmental loss of Phox2a results in deficient spinoparabrachial connections and a loss of sensitivity to noxious stimuli.

INTRODUCTION

In vertebrates, somatosensory information about noxious stimuli is carried from peripheral nociceptors to the brain via spinal projection neurons collectively known as the anterolateral system (AS), which also carries temperature and itch information. The brain regions innervated by nociceptive AS neurons interpret the transmitted signals as pain—a sensation endowed with discriminative and affective components that, respectively, convey the identity, location, and intensity of the stimulus as well as elicit behavioral responses driven

by arousal and aversion (Melzack and Casey, 1968). Since the molecular identity of AS neurons remains unknown, insights into the functional logic of nociceptive information relay from the periphery to the brain remain limited.

Prominent AS targets include the ventroposterolateral thalamus (VPL) (Gauriau and Bernard, 2004; Willis et al., 1979), which relays somatotopically organized nociceptive information (Guilbaud et al., 1980) to the primary somatosensory cortices, and the parabrachial nucleus (pB) (Bernard et al., 1995), which is considered to mediate affective components of pain by relaying noxious information to the amygdala (Han et al., 2015), and via the medial thalamus, to the prefrontal cortex (Bourgeois et al., 2001). Clinical evidence supports the division between discriminative and affective dimensions of pain, as prefrontal lobotomy (Freeman and Watts, 1948) and insular cortex-related pain asymbolia (Berthier et al., 1988; Rubins and Friedman, 1948) result in the discriminatory nature of noxious stimuli being appreciated in the absence of the negative affect. The critical role of the AS in relaying both discriminative and affective components of nociception to its brain targets is suggested by the effects of lesions to the spinal anterolateral tract (Spiller and Martin, 1912).

The anatomy of AS neurons is well known in rodents, where they are found principally in laminae I and V and the lateral spinal nucleus (LSN) of the spinal dorsal horn (Davidson et al., 2010; Kitamura et al., 1993). Lamina I AS neurons have small receptive fields (Willis et al., 1974) and respond to specific classes of stimuli and their modalities (e.g., temperature, itch, mechanical versus thermal pain) (Andrew and Craig, 2001; Craig and Serrano, 1994), which are relayed to targets thought to mediate discriminatory responses such as the VPL thalamus. Lamina V/LSN AS neurons, in contrast, have broad receptive fields and wide dynamic ranges of receptivity (Craig, 2003b), and their physiology corresponds poorly with the qualitative descriptions of pain (Craig, 2004). Based on their prominent projections to the dorsal pB (Feil and Herbert, 1995) and medial thalamus (Gauriau and Bernard, 2004), lamina V/LSN neurons likely transmit the affective and motivational dimensions of pain. These AS neuron functions are in line with substance-P receptor (NK1R)-directed AS neuron ablation, resulting in analgesia (Cameron et al., 2015; Mantyh et al., 1997). Recently developed genetic tools have uncovered the identity of interneurons that gate transmission of innocuous sensations to AS neurons (Duan et al., 2014; Petitjean et al., 2019), but genetic access to AS neurons has been elusive. Ablation of *Tachykinin1* (*Tac1*)-expressing spinal interneurons and pB-innervating AS neurons (Huang et al., 2019) produced behavioral deficits consistent with the loss of supraspinal transmission of nociceptive information without affecting the function of spinal nocifensive reflexes. Despite these advances, the genes expressed selectively in AS neurons remain unknown.

Developmental gene expression has been instrumental in studying locomotor circuits of the ventral spinal cord (Arber, 2012; Goulding, 2009) and may also be useful in accessing dorsal spinal cord somatosensory circuits. The dorsal spinal cord is divided into molecularly distinct neural precursor domains, whose link to adult neuronal classes remains obscure (Lai et al., 2016). Spinothalamic neurons express the transcription factor *Lmx1b* (Szabo et al., 2015), a marker of the putative projection neuron domain dI5, also expressed in other dorsal inter-neuron classes. In contrast, the Paired-like homeobox 2a (*Phox2a*) transcription factor

is a more selective, albeit transient, marker of developing dI5 neurons (Ding et al., 2004) and, thus, a potential selective label of AS neurons.

Here, we report that transient embryonic expression of *Phox2a* in spinal neurons defines the identity of several AS projection neuron classes. We also reveal a developmental diversity of AS neurons and show that a loss of *Phox2a* impairs AS neuron innervation of their brain targets, resulting in attenuated supraspinal responses to noxious stimuli. Furthermore, we show that the molecular identity of *Phox2a* AS neurons is conserved in the developing human spinal cord.

RESULTS

Spinal *Phox2a*^{Cre} Neurons Reside in Lamina I, Lamina V, and LSN

Mouse *Phox2a* and its proxy, bacterial artificial chromosome (BAC) transgene *Phox2a*^{GFP}, are expressed embryonically and perinatally in the superficial and deep dorsal horn, where many AS neurons reside (Allen Institute for Brain Science, 2008; GENSAT, 2008). In order to label these neurons in adults, we created the transgenic *Phox2a*^{Cre} mouse line by inserting a Cre-poly(A) minigene into the BAC RP23–333J21 (GENSAT, 2008), at the *Phox2a* ATG codon (Figure 1A), and assessed Cre expression via the Cre-dependent tdTomato (tdT) reporter *R26*^{LSL-tdT} (Ai14). Adult *Phox2a*^{Cre}; *R26*^{LSL-tdT} mice showed tdT expression throughout the rostrocaudal length of the spinal cord in dorsal horn neurons, principally in lamina I (Figure 1B) and lamina V/LSN (Figures 1B and S1A), as well as in spinal accessory nerve (mXI) motor neurons (Figure S1A). Although rare, large “antenna”-like neurons were also found in laminae III/IV (Figure S3) (Marshall et al., 1996). *Phox2a* and tdT are expressed throughout embryogenesis, but *Phox2a* expression is absent in adults (Figures 1C–1E). While tdT expression is specific to cells expressing *Phox2a*, only 33% of lamina V/LSN *Phox2a* cells (*Phox2a*^{Deep}) express tdT at embryonic day (E)16.5, while 82% of lamina I cells (*Phox2a*^{LamI}) do. Similar proportions were observed at E18.5 (Figure S1B), suggesting that the *Phox2a* BAC may be missing some enhancer sequences necessary for *Phox2a* expression. Together, these data constitute evidence that *Phox2a*^{Cre} can be used to trace the fate of *Phox2a*-expressing spinal neurons.

Spinal *Phox2a*^{Cre} Neurons Innervate AS Targets

To reveal the connectivity of spinal *Phox2a*^{Cre} neurons, we restricted *Phox2a*^{Cre}-driven reporter expression to the spinal cord using the Cre-Flp recombinase-dependent reporter *R26*^{FSF-LSL-tdT} (Ai65) combined with the caudal neural tube-specific Flp recombinase mouse line *Cdx2*^{FlpO} (Britz et al., 2015) to generate *Phox2a*^{Cre}; *Cdx2*^{FlpO}; *R26*^{FSF-LSL-tdT} mice (Figure 2A). To validate this genetic intersection, we compared cellular tdT reporter expression between adult *Phox2a*^{Cre}; *R26*^{LSL-tdT} mice (Figures 2B–2F and S2E–S2H) and *Phox2a*^{Cre}; *Cdx2*^{FlpO}; *R26*^{FSF-LSL-tdT} mice (Figures 2B'–2F' and S2E'–S2H'). In the brain, *Phox2a*^{Cre} drove cellular tdT expression in motor and autonomic nuclei (Figures 2B–2E and S2A–S2H), which was not observed in *Phox2a*^{Cre}; *Cdx2*^{FlpO}; *R26*^{FSF-LSL-tdT} mice (Figures 2B'–2E' and S2E'–S2H'). In the caudal spinal cord of *Phox2a*^{Cre}; *Cdx2*^{FlpO}; *R26*^{FSF-LSL-tdT} mice, however, the cellular expression of tdT+ expression was preserved (Figures 2F and 2F'), allowing us to map axonal trajectories and brain targets of spinal *Phox2a*^{Cre} neurons.

In *Phox2a^{Cre}*; *Cdx2^{FlpO}*; *R26^{FSF-LSL-tdT}* mice, tdT+ axons were observed in the lateral funiculus in a distribution similar to previous reports of lamina I spinofugal axon locations (Apkarian et al., 1985; McMahon and Wall, 1983) (Figure 2E'). We observed tdT+ axons in known AS targets such as the globus pallidus (GP; Figure 2G); VPL and posterior (Po) thalamus (Figures 2H and S2I); mediodorsal thalamus (MD; Figure 2I); the posterior triangular thalamus (PoT) and anterior pretectal nucleus (Figure S2K); the deep layers of the superior colliculus, possibly within the orientation barrels (Masullo et al., 2019) (Figure 2J, indicated by white arrowheads); periaqueductal gray (PAG; Figure 2K); the pB (Figures 2M and 2N); the nucleus of the solitary tract (NTS; Figure 2P); the locus coeruleus (LC; Figure 2C'); and the caudal ventrolateral medulla (CVLM; Figure 2D'). These termini colocalized with the presynaptic marker vGluT2, suggesting that they were glutamatergic synapses (Figures 2Q and 2Q'). Within the pB, the dorsal-lateral (pBdl), central-lateral (pBcl), and internal-lateral (pBil) subnuclei and regions surrounding the external-lateral (pBel) contained many tdT+ axons, while the superior-lateral (pBsl) and medial (pBm) subnuclei contained fewer axons (Figures 2M, 2N, S2M, and S2N). Consistent with previous reports, the pBel received very limited spinal innervation (Figures 2N, S2E, and S2N) (Bernard et al., 1995). Additionally, spinal *Phox2a^{Cre}* axons were also seen in brain regions not previously thought to receive direct AS innervation, such as the granular layers of the cerebellum ("gr" in Figure 2L), the vestibular nuclei (Figure 2O), the posterior hypothalamus near the A11 dopaminergic cell group (Figure S2J), and a region of the retrorubral area/dorsal-medial substantia nigra (Figure S2L). Thus, spinal *Phox2a^{Cre}* neurons innervate brain regions predominantly involved in autonomic regulation and homeostasis such as the pBdl, NTS, and CVLM, as well as nociceptive areas VPL, PAG, and pBil.

Spinal *Phox2a* Neurons Are Predominantly AS Neurons

Next, we determined the fraction of *Phox2a* neurons that are AS neurons. Adult *Phox2a^{Cre}*; *R26^{LSL-tdT}* mice were injected unilaterally with Fluoro-Gold (FG) in the VPL thalamus (Figure 3A) and with CTb-488 in the pB (Figure 3B). After 7 days, we examined the proportion of spinal neurons labeled with either or both tracers (Tracer+) that were also tdT+, sampled at all spinal cord levels (1,023 FG+, 6,620 CTb-488+, and 3,345 tdT+ cells from 7 mice). We focused on the cervical spinal cord, as spinothalamic neurons are relatively sparse in the mouse caudal spinal cord (Davidson et al., 2010). Overall, *Phox2a^{Cre}* labeled similar ratios of AS neurons traced from the VPL and the pB (26.9% ± 5.0% and 19.7% ± 4.3%, respectively; Figures 3C and 3D; n = 7). Consistent with the commissural nature of lamina I AS neurons, many *Phox2a^{Cre}* AS neurons were localized to the contralateral lamina I (Figures 3E, 3F, 3J, and 3K), in contrast to lamina V/LSN (Figures 3E, 3G, 3H, and 3I) where neurons were frequently seen labeled only with retrograde tracer. At least 20% of lamina V/LSN and approximately half of lamina I AS neurons, therefore, express *Phox2a^{Cre}*. Additionally, a bias in tdT expression to contralaterally projecting lamina I AS neurons suggests that *Phox2a^{Cre}* neurons may be involved in the localization of noxious stimuli (Figure 3K).

Contrarily, most tdT+ neurons are AS neurons, regardless of type: in our most comprehensive injections of tracer into the pB and VPL, we reached a labeling ceiling of ~80% of lamina V/LSN tdT+ neurons bilaterally and as much as 100% of lamina I tdT+

neurons, suggesting that all spinal *Phox2a^{Cre}* neurons contribute to the AS (Figures 3L–3N). Smaller fractions of tdT+ neurons were labeled by tracer injection into the pB or VPL, suggesting that *Phox2a^{Cre}* neurons represent multiple AS neuron types (Figure 3L versus Figures S3H–S3K). Although rare, antenna and lamina X tdT+ neurons were also predominantly AS neurons and tended to project contralaterally (Figures S3C–S3G). We also examined spinal projections to the MD thalamus (Figures S3L–S3R) as well as the cerebellar vermis (Figures S3S–S3Y) via retrograde tracer injection, which labeled fewer neurons than pB/VPL injections but also included tdT+ neurons. Clarke's column and ventral horn spinocerebellar neurons did not express tdT, suggesting that these canonical spinocerebellar neuron types are not derived from *Phox2a*-expressing neurons. In the hindbrain, pB, VPL, and MD tracer injections also labeled tdT+ neurons in the CVLM, parvocellular reticular nucleus (PARN), and spinal trigeminal lamina I/paratrigeminal region (Figures S3Z–S3CC), suggesting shared functions with spinal *Phox2a^{Cre}* neurons.

Heterogeneity of Spinal *Phox2a* Neuron Migration, Sensory Afferent Interaction, and Birth Time

We next studied the cellular and molecular events underlying *Phox2a* neuron development. First, we followed their migration via *Phox2a* and tdT expression in *Phox2a^{Cre}; R26^{LSL-tdT}* spinal cords throughout embryonic development. *Phox2a* neurons first appear at E10.5 in the cervical region and begin expressing tdT 1 day later (Figure 4A). At E12.5, three *Phox2a* populations are evident: *Phox2a*+tdT+ (*Phox2a^{LamI}*) neurons ventrolateral to the nascent dorsal horn, and two medial populations consisting of *Phox2a*+tdT+ and those expressing only tdT. At E13.5, *Phox2a^{LamI}* neurons disperse on the surface of the nascent superficial dorsal horn tangentially, while deeper *Phox2a* neurons (*Phox2a^{Deep}*) acquire positions that correlate with tdT expression: *Phox2a^{Deep}* tdT+ neurons remained ventrolateral to the dorsal horn, while *Phox2a^{Deep}* tdT– neurons accumulated above the central canal. At E14.5, *Phox2a^{Deep}* tdT– neurons migrate laterally and eventually become intermingled with *Phox2a^{Deep}* tdT+ neurons at E15.5, achieving their final configuration (Figure S4A). These results suggest the existence of at least three distinct migratory paths of *Phox2a* neurons.

As the tangential dispersal of *Phox2a^{LamI}* neurons within the dorsal horn occurs at the time of primary afferent innervation, we asked how these two events are related. Prior to their entry into lamina I, *Phox2a^{Cre}* neurons project processes toward the dorsal root entry zone (Figures S4C and S4D) and form appositions with TrkA+ primary afferents at E13.0 as *Phox2a^{LamI}* neurons begin migrating dorsally (Figures 4B and S4B), resulting in E13.5 *Phox2a^{LamI}* neurons becoming encased in TrkA+ afferents (Figures S4E and S4F). To determine whether TrkA+ axons contribute to *Phox2a^{LamI}* neuron positioning, we examined the location of *Phox2a* neurons in *TrkA* null (*TrkA^{-/-}*) mouse embryos, in which most TrkA+ afferents are absent (Smeyne et al., 1994). Compared to controls, the number of *Phox2a^{LamI}* neurons in *TrkA^{-/-}* embryos was approximately halved (Figures 4C–4E), suggesting that TrkA+ afferents may interact with migrating *Phox2a* neurons. Although we found no significant effects of TrkA axonal loss on *Phox2a^{Deep}* neurons, their count tended to increase, suggesting that *Phox2a^{LamI}* neurons fail to migrate and stall at the base of the forming dorsal horn (Figures 4C–4E).

To determine whether spinal Phox2a neuron diversity and migration patterns correlate with the time of their birth, we injected pregnant *Phox2a^{Cre}; R26^{LSL-tdT}* mice with bromodeoxyuridine (BrdU) at E9.5, E10.5, and E11.5 and examined strong BrdU co-staining with Phox2a or tdT in E16.5 *Phox2a^{Cre}; R26^{LSL-tdT}* embryos (Figures 4F–4M and S4R–S4T). Nearly all Phox2a^{LamI} neurons were born at E9.5, while Phox2a^{Deep} neurons were born between E9.5 and E10.5, with very few born later. Furthermore, E11.5 Phox2a neurons that give rise to Phox2a^{LamI} neurons (Figure 4A) are also born at E9.5 (Figures S4G–S4M). Given the differential expression of Phox2a and tdT in Phox2a^{Deep} cells, we developed a model in which Phox2a^{LamI} and antenna neurons are born first, followed by Phox2a^{Deep} tdT+ (Phox2a^{DeepEarly}), while Phox2a^{Deep} tdT– neurons are born last (Phox2a^{DeepLate}) but not beyond E11.5 (Figures 4N and S4N–S4Q). More generally, our data show that AS neurons constitute one of the earliest born spinal neuron populations.

The Molecular Identity and Specification of Spinal Phox2a Neurons

To uncover the molecular pathways controlling Phox2a AS neuron specification, we studied their expression of neuronal identity determinant genes, identified transcription factor programs that specify them, and sought molecular markers that subdivide them. Spinal Phox2a expression begins at E9.5 and is restricted to spinal accessory motor neurons (Figures S5A and S5B). Non-motor neuron Phox2a expression is first visible at E10.5 in Lmx1b+ (dI5) post-mitotic neurons, which do not express the progenitor markers *Ascl1* or *Pax7* or the dI1, dI3, or dI4/6 transcription factors *Lhx2*, *Isl1*, or *Pax2*, respectively, but which do express dI5 transcription factors *Lbx1*, *Tlx3*, and *Brn3b/Pou4F2* and the commissural neuron guidance receptors *Robo3* and *DCC* (Figures 5A, 5B, S5C, and S5D). These findings demonstrate that non-motor neuron spinal Phox2a cells are predominantly commissural dI5 neurons.

Since spinal Phox2a neurons develop from dI5 embryonic neurons, and since dI5 neuron identity is specified by the transcription factor *Ascl1* while *Ptf1a* suppresses dI5 identity and induces the neighboring dI4 identity (Glasgow et al., 2005; Helms et al., 2005), we assessed whether Phox2a expression was altered in *Ascl1* null (*Ascl1^{GFP/GFP}*) and *Ptf1a* null (*Ptf1a^{CRE/CRE}*) spinal cords. Compared to littermate controls, virtually no Phox2a neurons were found in E11.5 *Ascl1^{GFP/GFP}* spinal cords, while additional Phox2a neurons were found in E11.5 and E14.5 *Ptf1a^{CRE/CRE}* embryos (Figures 5C–5F, S5E, and S5F). To determine whether *Ascl1* and *Ptf1a* transcription factors control Phox2a expression directly or indirectly, we analyzed chromatin immunoprecipitation sequencing (ChIP-seq) data (Borromeo et al., 2014) for *Ascl1* and *Ptf1a* binding to the *Phox2a* locus. A genomic region (*ePhox2a*) located >30 kb downstream of the *Phox2a* transcription start site was bound by *Ascl1* and *Ptf1a*, but not the *Ptf1a* co-factor *Rbpj* or *Prdm13*, both of which act to repress dI5 and promote dI4 identity (Figure S5G) (Chang et al., 2013; Hori et al., 2008). To test the ability of *Ascl1*, *Ptf1a*, and *Prdm13* to regulate Phox2a through *ePhox2a*, we co-electroporated plasmids encoding these proteins together with a plasmid containing an *ePhox2a* activity reporter (*ePhox2a:GFP*; Figure S5H) into chick spinal neuron progenitors and monitored GFP expression. *ePhox2a:GFP* alone directed GFP expression in a small number of neurons located within the dI5 domain (Figures 5G and S5I). Ectopic *Ascl1* (but not ectopic *Ptf1a* or *Prdm13*) dramatically increased the number of GFP+ cells (Figures 5H–

5J). Furthermore, Phox2a expression was entirely abolished in *Lmx1b*^{-/-} E11.5 mouse spinal cords (Figure S5J). Together, these data suggest that *Ascl1* and *Lmx1b* are required for Phox2a expression, with *Ascl1* acting directly through a 3' enhancer, while *Ptf1a* represses Phox2a transcription (Figure 5K).

Given that Phox2a labels a set of AS neurons, we sought to identify other genes expressed within AS neurons using available single-cell RNA-sequencing (RNA-seq) data from E9.5–E13.5 mouse spinal cords (Delile et al., 2019). Since Phox2a neurons are a subset of *Lmx1b*-expressing dI5 neurons, we performed uniform manifold approximation and projection (UMAP) dimensionality reduction analyses on two cohorts of dI5 neurons: (1) those found at all time points (E9.5–E13.5; 2,614 neurons; Figure 5L) and (2) an earlier subset of *Lmx1b* neurons (E9.5–E11.5; 186 neurons; Figure 5N) in order to attempt to separate the early dI5 neurons (pre-lamina I neurons) into subsets. From these, we were able to isolate clusters of dI5 neurons enriched for Phox2a+ neurons (Figures 5M, 5P, S5K, and S5L), as well as an early dI5 cluster enriched for *Tac1* (Figures 5O and S5L). Top enriched transcripts for each cluster are listed in Table S1. Select transcripts were then validated using immunohistochemistry and RNAscope *in situ* hybridization in E11.5 and E16.5 spinal cords. At E11.5, Phox2a neurons were enriched for the expression of *Nms*, *Tm4sf4*, *Scn9a*, and *Zim1* mRNAs (Figures 5Q and 5R), which remained expressed in E16.5 Phox2a^{LamI} neurons (Figures 5T and 5U), providing further support that the E11.5 Phox2a cells populate lamina I. Other dI5-enriched transcripts and proteins, *Syt4*, *Pdzrn3*, *Shox2*, and *Pou6F2*, were also highly co-expressed with Phox2a but were less specific to Phox2a neurons (Figures S5M–S5P). *Tac1*, however, was expressed in a complementary set of dI5 and lamina I neurons (Figures 5Q, 5R, 5T, and 5U) in line with the separation of dI5 neurons into two types suggested by our UMAP analyses, potentially describing a molecular division of superficial dorsal horn AS neurons (Figures 5S and 5V). Together, these experiments reveal the cellular and molecular mechanisms of AS neuron specification and unravel an array of AS-enriched mRNAs.

Phox2a Is Required for AS Neuron Development

Given the requirement of Phox2a for normal LC development (Morin et al., 1997), we hypothesized that its loss may also impact the development of spinal Phox2a neurons. As *Phox2a* null mice do not survive beyond birth, we used the *Hoxb8*^{Cre} mouse line to ablate *Phox2a* selectively in the caudal nervous system and a Cre reporter (*R26*^{LSL-tdT}) to visualize AS axons (Figure S6A) (Bourojeni et al., 2020; Witschi et al., 2010), producing Phox2a^{cKO} (*Hoxb8*^{Cre}; *Phox2a*^{f/f}; *R26*^{LSL-tdT}) and control (*Phox2a*^{f/f} or *Hoxb8*^{Cre}; *Phox2a*^{+/+}; *R26*^{LSL-tdT}) adult mice. Examination of tdT axons in adult Phox2a^{cKO} and control mice revealed that, while most spinofugal targets were normally innervated in Phox2a^{cKO} mice (Figure S6C), a dramatic loss of tdT axons was observed in the pBil (Figures 6A and 6B; additional examples are given in Figure S6B). Using retrograde tracing from the pBil of adult mice, we demonstrated that control and Phox2a^{cKO} mice had comparable numbers of cervical lamina I and lamina V/LSN neurons projecting to the pB (Figures S6D–S6F). In the lumbar spinal cord (within the *HoxB8*^{Cre} expression domain), however, while the tracer-labeled lamina I neuron number was unchanged in Phox2a^{cKO} mice (Figures 6C and 6D), the number of Tracer+ ipsilateral and contralateral lamina V/LSN neurons was decreased by

approximately 75% (Figures 6C and 6E). To investigate cellular changes leading to these connectivity phenotypes, we localized *Phox2a* mRNA in E16.5 control and *Phox2a*^{cKO} embryos, likely made possible by the persistence of the truncated *Phox2a* transcript. This analysis revealed similar numbers of *Phox2a* neurons in control and *Phox2a*^{cKO} E16.5 mice (12.6 ± 3.7 cells per section, $n = 4$; and 16.6 ± 1.5 cells per section, $n = 4$, respectively; $p = 0.089$, unpaired t test), although *Phox2a*^{Deep} neurons were displaced medially (Figures 6H and 6I), arguing that these cells are present in *Phox2a*^{cKO} mice but may be dysfunctional. *Phox2a* mRNA expression in *Phox2a*^{cKO} mice appeared elevated compared to that in controls, suggesting that *Phox2a* may negatively regulate its own expression.

To understand the molecular underpinnings of these phenotypes, we compared the expression of *Phox2a* AS neuron-enriched mRNAs (Figure 5) in control and *Phox2a*^{cKO} mice. Only the expression of *Tm4sf4*, a gene encoding a protein implicated in cellular differentiation, was affected by *Phox2a*^{cKO} mutation in E11.5 dI5 neurons and E16.5 lamina I neurons (Figures 6F, 6G, 6J, 6K, and S6G). Given the peptidergic heterogeneity of lamina V/LSN neurons (Leah et al., 1988), we also monitored the expression of neuromodulatory peptides and receptors in presumptive *Phox2a*^{Deep} neurons in E16.5 *Phox2a*^{cKO} and control spinal cords. Expression of genes encoding lamina V/LSN-enriched peptides *Sst* (somatostatin) and *Crh* (corticotrophin-releasing hormone) were reduced in *Phox2a*^{cKO} mice, while the expression of other *Phox2a* neuron-enriched transcripts remained unaffected (Figures 6L, 6M, S6K, and S6L). We also monitored the expression of selected neuromodulatory genes in lamina I neurons and found elevated expression of *Vip* in *Phox2a*^{cKO} mice (Figure S6J); however, glutamatergic identity of *Phox2a* neurons was not changed (Figures S6H and S6I). Consistent with this, mRNAs encoding neuropeptides associated with inhibitory neurons were expressed sparsely among *Phox2a*^{Deep} neurons (Figure S6M). Together, these results demonstrate that *Phox2a* is essential for the normal axonal connectivity and migration of many AS neurons, as well as for their neuromodulatory identity.

Spinal *Phox2a* Loss Impairs Supraspinal Nocifensive Behaviors

Given the central role of the AS in supraspinal nociceptive signal relay, we reasoned that defects in spinoparabrachial connectivity and *Phox2a*^{Deep} neuromodulatory peptide expression in *Phox2a*^{cKO} mice might result in impaired nocifensive behaviors that are evoked by supraspinal circuits, with minimal effect on spinally mediated behaviors. Indeed, thermal and mechanical nociceptive reflex assays did not reveal any differences between control and *Phox2a*^{cKO} mice (Figures 6N–6P). Thermal preference to innocuous and noxious temperatures (Figures S6T–S6V) and behaviors evoked by light touch in the adhesive removal test (Figures 6Q and S6N) were also not affected by the *Phox2a*^{cKO} mutation. However, using a battery of behavioral assays requiring supraspinal transmission of noxious information, *Phox2a*^{cKO} mice showed deficits in hindpaw licking evoked by noxious stimuli—a nocifensive behavior requiring ascending spinal projections. Notable deficits emerged in the 53°C hot-plate assay, which monitors noxious heat sensitivity (Figures 6R, S6O, and S6Q); in the acetone assay, which monitors responses to cooling (Figures 6T and S6S); and following noxious mechanical stimulation (Figure 6U). Reflex-mediated, hot-plate-evoked behaviors remained unchanged (Figures 6S and S6P). We

attempted to measure nocifensive behaviors in the cold-plate assay, but neither control nor Phox2a^{cKO} mice responded (Figure S6R). In addition, Phox2a^{cKO} mice also exhibited less licking of hindpaws injected with the TRPV1 and TRPA1 agonists capsaicin and formalin, respectively, although the late/tonic phase of post-formalin injection licking was unaffected (Figures 6V–6X). Together, these results show that a loss of Phox2a during development disrupts AS neuron innervation of the pB, disrupts their molecular differentiation and concomitantly affects the supraspinal aspects of a variety of nocifensive behaviors associated with AS function.

Phox2a Neuron Molecular Identity Is Conserved in the Developing Human Spinal Cord

Given that little is known about the molecular identity of human spinal neurons, we also asked whether Phox2a expression in the developing human spinal cord might allow insights into human AS development. We thus examined the expression of Phox2a protein in human spinal cords at developmental ages comparable to mouse mid-gestation: two at gestational week (GW)7.3 and one each at GW7.4, GW8.0, and GW8.4, three of which are shown in Figures 7A and S7 (Altman and Bayer, 2001). At GW7.3, Phox2a neurons (identified using a commercial Phox2a antibody; Figure S7C) were found in the superficial dorsal horn adjacent to TrkA⁺ fibers (Figures 7B', S7A, and S7B), in deeper laminae (Figure 7B''), and near the roof plate (Figure 7B'''), resembling the location of mouse Phox2a^{LamI} and Phox2a^{Deep} neurons. Human spinal Phox2a neurons co-expressed Lmx1b and Lbx1, but not Pax2 or Tlx3 (Figures 7B, S7A, and S7B). A previous study that examined Tlx3 expression in the human spinal cord did show its expression in the putative dI5 domain at GW5, although it was not compared to Phox2a expression (Marklund et al., 2014). As in mice, human Phox2a expression appeared weaker in older spinal cords (GW8.4; Figures 7A and S7B). Together, these data suggest that the spinal Phox2a neuron developmental program is evolutionarily conserved and that Phox2a expression is a molecular feature of developing human AS neurons.

DISCUSSION

Spinal neurons that express Phox2a^{Cre} during their development constitute a major tributary of the AS. Our studies reveal their developmental heterogeneity and requirement for normal nociception, as well as provide insights into a molecular logic that underlies their functions.

Diversity of AS Neuron Development

Nearly all spinal Phox2a^{Cre} neurons can be retrogradely labeled from the VPL thalamus and the pB, indicating that Phox2a is a genetic marker of a subpopulation of AS neurons. This has allowed us to investigate the development of AS neurons, revealing three neuronal classes that arise from embryonic dI5 neurons: Phox2a^{LamI}, Phox2a^{DeepEarly}, and Phox2a^{DeepLate}. A recent study argues that some AS neurons express *Tac1* (Huang et al., 2019); our molecular profiling suggests that the early population of dI5 *Lmx1b*⁺ *Tac1*⁺ neurons likely gives rise to *Tac1*⁺ AS neurons, that this population does not overlap with early-born Phox2a-expressing dI5 neurons, and that there are at least two molecularly distinct Lamina I AS neuron subpopulations: *Phox2a*⁺ and *Tac1*⁺. Contrary to the notion that spinal neurons are born in a ventral-to-dorsal order (Nornes and Carry, 1978), superficial dorsal

horn Phox2a neurons are born concurrently with motor neurons, as suggested recently for spinofugal neurons (Nishida and Ito, 2017). *Ascl1* (expressed in dI5 progenitors) and *Ptf1a* (expressed in dI4 progenitors) were previously shown to promote and inhibit dI5 neuron fates, respectively (Glasgow et al., 2005; Helms et al., 2005). Our data demonstrate that this may occur via action at a 3' *Phox2a* enhancer defined in this study. The stereotyped birth order of Phox2a AS neurons raises the possibility that it is orchestrated by transcription factors involved in the temporal competence of *Ascl1*-expressing progenitors, as in the cerebral cortex and retina (Kohwi and Doe, 2013).

Following birth and early specification, Phox2a^{LamI}, Phox2a^{DeepEarly}, and Phox2a^{DeepLate} AS neurons migrate along distinct tangential and radial trajectories. The contacts between afferent axons and Phox2a^{LamI} neurons may be important for the settling of lamina I neurons in a somatotopic order corresponding to their dermatome-specific sensory afferents (Willis et al., 1974). At the molecular level, the neuronal migration cue Reelin likely mediates the radial migration of Phox2a^{Deep} neurons, since its intracellular signaling effector Dab1 is required for normal positioning of lamina V/LSN neurons (Yvone et al., 2017). Conversely, Netrin1 in the nascent dorsal horn prevents the premature ingrowth of primary afferents (Watanabe et al., 2006), and the netrin-1 receptor DCC is required for the normal entry of Phox2a^{LamI} neurons into the dorsal horn (Ding et al., 2005). Thus, netrin signaling likely contributes to the interplay between sensory afferents and Phox2a^{LamI} neurons, while Phox2a^{Deep} neuron migration might rely on reelin signaling.

Phox2a Is Required for the Terminal Differentiation of AS Neurons

Phox2a-expressing neurons are present in normal numbers in embryonic Phox2a^{cKO} spinal cords, suggesting that Phox2a is not required for their early specification or survival. However, *Phox2a* mutation results in the loss of *Tm4sf4* and gain of *Vip* expression in Phox2a^{LamI} neurons, indicating that Phox2a is required for their molecular differentiation and, thus, possibly their function, despite apparent normal target connectivity. In contrast, lamina V/LSN Phox2a neurons are more dramatically affected, as nearly 75% of lamina V/LSN AS neurons fail to innervate the pB in Phox2a^{cKO} mice. This indicates that Phox2a is expressed in the vast majority of lamina V/LSN neurons, in agreement with our observation that *Phox2a*^{Cre} under-reports Phox2a expression in many of these neurons. Aberrant Phox2a^{Deep} neuron position in Phox2a^{cKO} mice, similar to that observed for lamina V and LSN neurons in Reelin signaling-deficient mice (Wang et al., 2012; Yvone et al., 2017), suggests that Phox2a may be required for expression of Reelin signaling genes. Together with the observation that *Phox2a* mutation also results in the loss of neuropeptide expression in Phox2a^{Deep} neurons, these defects argue that Phox2a specifies the terminal differentiation of a subset of AS neurons, and its absence likely impairs their function.

Phox2a AS Neuron Function in Supraspinal Nociception

The transmission of noxious and thermal information is a major function of the AS, and adult spinal Phox2a neuron morphologies, laminar organization, and their brain targets are consistent with such a function. The normal hindpaw adhesive-tape-evoked behaviors in Phox2a^{cKO} mice are consistent with the notion that light touch sensation is not a function of the AS (Hyndman and Wolkin, 1943). Phox2a^{cKO} mice also have normal spinal nocifensive

reflexes, indicating that neither local reflex circuitry nor the descending pathways that modulate these behaviors (Ren and Dubner, 2009) depend on normal AS function. The apparently normal temperature preference of Phox2a^{CKO} mice may result from normal thermosensation in the forepaws and head, which is processed in the upper cervical spinal cord rostral to *Hoxb8*^{Cre} expression (Bourojeni et al., 2020; Witschi et al., 2010).

In comparison, Phox2a^{CKO} mice exhibit a reduction in the frequency and duration of behaviors evoked by the transmission of noxious information from the spinal cord to the brain, a function likely carried out by Phox2a AS neurons. While lamina I AS neurons have been proposed to transmit sensory-discriminative information and are likely to be impaired in Phox2a^{CKO} mice, a lack of motivation to respond to noxious stimuli—likely due to defects in Phox2a lamina V/LSN neurons—prevents us from testing this hypothesis. Our data, together with earlier studies, implicate lamina V/LSN neurons in directing motivated nocifensive behaviors via the spino-pBil-medial thalamus pathway (Bourgeois et al., 2001; Deng et al., 2020). Our observations are also in line with those made in mice with a loss of Tac1 spinal neurons (Huang et al., 2019), in that approximately 20% of Phox2a^{Deep} neurons express *Tac1*, and so their loss may affect the transmission of motivational nociceptive information from the spinal cord to the brain. However, a loss of Tac1 interneurons that control the function of Phox2a^{Deep} neurons may also contribute to the observed phenotypes. At the molecular level, Phox2a^{CKO} mice show decreased expression of the neuropeptides *Sst* (Leah et al., 1988) and *Crh*, normally enriched in Phox2a^{Deep} neurons of lamina V/LSN. Given the role of CRH in stress responses, *Crh*-expressing Phox2a^{Deep} neurons may convey motivational information linked to noxious stimuli.

The Molecular Logic of the AS

Although *Phox2a*^{Cre} labels a subpopulation of Phox2a neurons, we are compelled to draw some general inferences about the significance of Phox2a expression in AS neurons. Supraspinal Phox2a lineage-derived neurons exist in a variety of autonomic circuits, raising the question of whether these may be functionally intertwined with Phox2a AS neurons. Two lines of thought shed some light on this. First, Phox2a and its closely related transcription factor Phox2b specify the development of neurons afferent to medullary visceral reflex circuits that control many autonomic functions implicated in homeostasis (Brunet and Pattyn, 2002). Our genetic tracing experiments reveal that Phox2a AS neurons participate in this connectivity logic by innervating brain stem autonomic regions such as the NTS and CVLM, as well as higher autonomic regulatory regions such as the pB. Second, because pain motivates behaviors that correct homeostatic changes, it has been proposed as a “homeostatic emotion” (Craig, 2003a). In light of this, the AS can be viewed as a pathway signaling deviations from homeostasis, such as changes in skin temperature, or the presence of noxious or pruritogenic stimuli, to brain regions that trigger compensatory autonomic responses (e.g., CVLM) or drive compensatory behavioral responses such as licking or scratching (e.g., pB). Given this, Phox2a AS neurons may specialize in transmitting somatic sensations with a motivational character such as cutaneous and deep pain, thermosensation, itch, visceral pain, nausea, and sexual arousal, all of which are abolished by anterolateral cordotomy in humans (Hyndman and Jarvis, 1940; Hyndman and Wolkin, 1943).

Our results suggest that the molecular identity of mouse *Phox2a* AS neurons is conserved in the developing human spinal cord, pointing to a conserved molecular logic of somatosensory circuit development, supported, in part, by the expression of *PHOX2A* in the human LC (Fan et al., 2018). A genetic proof of this idea remains out of reach because of the lack of obvious nociceptive or autonomic deficits in humans with *PHOX2A* mutations, which may be due to hypomorphic alleles (Nakano et al., 2001). Nevertheless, *PHOX2A* is a compelling molecular marker of human AS neurons and, given the effectiveness of cordotomy as a crude treatment of intractable chronic pain, a molecularly defined inactivation of a *Phox2a* AS neurons subpopulation could be its more refined iteration.

STAR★METHODS

Detailed methods are provided in the online version of this paper and include the following:

RESOURCE AVAILABILITY

Lead Contact—Further information and requests for resources and reagents should be directed to and will be fulfilled by the Lead Contact, Artur Kania (artur.kania@ircm.qc.ca).

Materials Availability—*Phox2a*^{Cre} mice are available from the Lead Contact upon request.

Data and Code Availability—The published article includes all datasets generated in this study. Single cell RNA-Seq data analyzed here was generated by Delile et al. (2019) and was obtained per their instructions from Array Express (<https://www.ebi.ac.uk/arrayexpress/>) with accession number “E-MTAB-7320.”

EXPERIMENTAL MODEL AND SUBJECT DETAILS

Mouse lines and *Phox2a*^{Cre} mouse line generation—Adult male and female mice, between 6–19 weeks of age, were used in this study. Sex ratios were kept as close to 1:1 as possible in all experiments, though not all experiments had the power to distinguish sex differences. Mice were kept on a 12 hour light: 12 hour dark cycle (light 6:00–18:00) with food and water provided *ad-libitum*. All procedures (except those involving *TrkA*^{−/−}, *Ptf1a*^{CRE} and *Ascl1*^{GFP} mice) were approved by the IRCM Animal Care Committee, using regulations and guidelines provided by the Canadian Council for Animal Care (CCAC). *TrkA*^{−/−} mouse use was approved by the Committee of Animal Care and Use of the National Cancer Institute, while the use of *Ptf1a*^{CRE} and *Ascl1*^{GFP} mouse lines (maintained on a mixed background of ICR and C57BL/6), was approved by the Institutional Animal Care and Use Committee at University of Texas Southwestern. *Phox2a*^{Cre} mice were generated at the IRCM where *Phox2a*-containing BAC RP23–333J21 (GENSAT, 2008) was modified by insertion of a Cre-PolyA sequence into the ATG site of *Phox2a* using GalK recombineering strategies (Warming et al., 2005). The Cre-containing BAC was injected into fertilized ova, and the resulting offspring were screened for genomic insertion of the BAC using Cre PCR. In total, we screened 230 pups, and were able to produce one founder from which all mouse lines containing *Phox2a*^{Cre} were derived. Genotyping was done by PCR for *Cre*, *FlpO*, *R26*^{LSL-tdT+} (Ai14), *R26*^{FSF-LSL-tdT+} (Ai65), *Phox2a*^{fl/fl} and *TrkA*^{−/−} as previously

described (Glasgow et al., 2005; Kim et al., 2008). The *Ptf1a^{CRE}* mouse line replaces the coding sequence for *Ptf1a* with that for *Cre* recombinase (Kawaguchi et al., 2002) and the *Ascl1^{GFP}* (*Ascl1^{tm1Reed/J}*) mouse strain replaces the coding sequence of *Ascl1* with that for *GFP* (Leung et al., 2007).

Generation of mice and mouse embryos—Mice containing the following transgenes or alleles were generated: *Phox2a^{Cre}*; *R26^{LSL-tdT/+}*, *Phox2a^{Cre}*; *Cdx2^{FlpO}*; *R26^{FSF-LSL-tdT/+}*, *Hoxb8^{Cre}*, *Phox2a^{f/f}*, *R26^{LSL-tdT/+}*, *Ascl1^{GFP/GFP}*, *Ptf1a^{Cre/Cre}*, and *TrkA^{-/-}* by breeding parents bearing one or more of the necessary alleles/transgenes. Vaginal plugs were checked daily at 6:00am, and the day of plug detection was noted as embryonic day 0.5 (e0.5). Mothers were anesthetised with a 0.3 mL intra-peritoneal injection of Ketamine/Xylazine solution. Embryos were dissected in ice-cold 1× phosphate-buffered saline (1× PBS), transferred to 4% paraformaldehyde in 1× PBS (4°C) and left to fix for two hours on a moving shaker (except *Ptf1a^{Cre/Cre}* and *Ascl1^{GFP/GFP}* embryos which were fixed for one hour). After fixation, embryos were washed briefly in 1× PBS, then cryoprotected in 30% sucrose for 1–2 days or until sunk. Embryos were harvested and fixed on the following embryonic days: *TrkA^{-/-}* on E14.5, *Ptf1a^{Cre/Cre}* and *Ascl1^{GFP/GFP}* both on E11.5 and E14.5, *Hoxb8^{Cre}*; *Phox2a^{f/f}*; *R26^{LSL-tdT/+}* on E11.5 and E16.5, and *Phox2a^{Cre}*; *R26^{LSL-tdT/+}* on E9.5, E10.5, E11.5, E12.5, E13.0, E13.5, E14.5, E15.5, E16.5 and E18.5.

Acquisition of human embryonic spinal cords—Human embryos were obtained with the parent's written informed consent (Gynaecology Hospital Jeanne de Flandres, Lille, France) with approval of the local ethic committee. Tissues were made available via the INSERM-funded Human Developmental Cell Atlas resource (HuDeCA) in accordance with the French bylaw (Good practice concerning the conservation, transformation and transportation of human tissue to be used therapeutically, published on December 29, 1998). Permission to use human tissues was obtained from the French agency for biomedical research (Agence de la Biomédecine, Saint-Denis La Plaine, France). Human embryo spinal cords were fixed by immersion for 12–24 hours in 4% paraformaldehyde in 0.12 M phosphate buffer, pH 7.4 (PFA) over night at 4°C. Samples were cryoprotected in a solution of 10% sucrose in 0.12 M phosphate buffer (pH7.2), frozen in isopentane at 50°C and then cut at 20 µm with a cryostat (NX70 Thermo Fisher). Spinal cords from five separate embryos were used in this study: two from G.W. 7.3, and one each from G.W. 7.4, 8.0 and 8.4.

METHOD DETAILS

Neuronal birthdating—Pregnant female mice were given an i.p. injection of BrdU on E9.5, E10.5, E11.5 or E12.5 and embryos were harvested and fixed at E11.5, E12.5, E13.5 or E16.5. The BrdU dose was 50 mg/kg for all time points except E9.5, where this dose produced ubiquitous BrdU+ immunoreactivity in the spinal cord and thus was reduced to 25 mg/kg.

Stereotaxic surgery—Prior to surgery mice were given 1 mg/kg buprenorphine for analgesia, then anesthetised using a mixture of 5% isoflurane in oxygen and maintained using 2% isoflurane in oxygen. Eyes were coated in eye ointment to prevent drying during

anesthesia. Prior to incision, the top of the head was shaved and decontaminated using an iodine solution. Mice were fitted into a stereotaxic frame with digital coordinate display and an incision was made longitudinally along the scalp to bare skull sutures. Injections were made via a hole drilled in the skull, which was made using medial-lateral and anterior-posterior coordinates for underlying brain regions as defined by the coronal Allen Brain reference atlas (Dong, 2008). Retrograde tracers (fluorogold or CTb-488) were injected using a 5 μ L Hamilton syringe fitted with a pulled glass needle backfilled with mineral oil, which were injected in the VPL thalamus (coordinates AP -1.7 , ML -2.0 , DV -3.2), the MD thalamus (AP -1.25 , ML -0.4 , DV -3.2), the cerebellar vermis (AP -6.2 , ML -0.8 , DV -2.0), or the parabrachial nucleus (AP -5.35 , ML -1.4 , DV -3.05), identified using the coronal Allen Brain reference atlas (Allen Institute for Brain Science, 2004). Injection volumes of 500 nL (fluorogold, 2%) were injected into the VPL and 300 nL (CTb-488, 1%) into the MD thalamus, cerebellum or parabrachial nucleus. The needle was left in place for 5 minutes before slowly withdrawing to prevent reflux. The incision was then stitched together using silk sutures and mice were allowed to recover under a heating lamp before being returned to their home cage. Mice were perfused at 7 days post-injection and spinal cords were dissected.

Mouse behavioral assays—R. B. R. performed all behavioral assays, and was blinded to genotypes. R. B. R. and M. B. analyzed video-recorded mouse behavior, though each experimenter analyzed equal numbers of mice from each sex and genotype per assay. Mice of both sexes were used in each behavioral assay. Mice from control and Phox2a^{CKO} groups were always littermates and the same sex, to prevent confounding effects of litter versus sex. Control and Phox2a^{CKO} groups thus always contained an equal proportion of mice from each sex, and the proportion of male to female mice within groups was kept as close to 50% as possible, constrained only by the number of Phox2a^{CKO} mice generated (at an expected rate of 12.5% in a given litter). Mice were habituated in a dedicated mouse behavior room for at least 30 minutes prior to onset of tests. Mice received no other treatments other than the test itself. Mice were habituated in a small plexiglass chamber measuring 4 cm long, 2.2 cm wide and 2.5 cm high for von Frey, radiant heat paw-withdrawal, acetone and adhesive removal tests. For the von Frey and acetone tests, the chambers were placed atop a perforated stainless-steel floor due to the need for physical hind paw manipulations. For the radiant heat paw-withdrawal and adhesive removal test, the chambers were placed atop a transparent glass sheet. For all other assays mice were habituated in their home cages. When necessary, all behavioral tests were filmed using an iPhone SE except for the temperature preference assay, where the video camera included in the apparatus was used.

The **von Frey test** involved using a set of nylon filaments (0.008, 0.02, 0.04, 0.07, 0.16, 0.4, 0.6, 1.0, 1.4 g) to stimulate the hind paw plantar surface of each mouse in order to determine the median force which produces a withdrawal reflex. Mice were tested with a series of filaments using the “up-down” method of Dixon, as described previously (Chaplan et al., 1994; Mogil et al., 1999), with an inter-trial interval of at least 5 minutes.

The radiant heat paw-withdrawal (**Hargreaves**) test involved stimulating the hind paw plantar surface from below with a focused beam of light (set to 10% maximum intensity of the machine) and verifying latency to withdraw either hind paw. Each hind paw was

stimulated eight times (16 total stimulations), and data was represented as the average of 16 withdrawal latencies, with an inter-trial interval of at least 2 minutes, performed as previously described (Hargreaves et al., 1988; Mogil et al., 1999).

The **hot water tail-withdrawal** test was performed as described previously (Mogil et al., 1999). Mice were placed in a small cloth pouch into which they entered voluntarily, the distal portion of the tail was dipped into a hot water bath maintained at $49 \pm 1^\circ\text{C}$ and the latency to withdraw the tail was recorded. Mice were tested three times with an inter-trial interval of at least 2 minutes, and data was represented as the average of 3 withdrawal latencies.

The **adhesive removal test** was performed as described previously (Bouet et al., 2009). Mice were tested on five consecutive days for the ability/motivation to remove an adhesive placed on the plantar surface of the hind paw. The adhesive was half of a 1.5 mL Eppendorf tube cap label, cut into a semicircle, and placed on the plantar surface. The latency to remove the label was recorded to the nearest minute, and these data were reported exactly as recorded (with only one test per day and no averaging between trials). If mice did not remove the adhesive within 30 minutes of the start of the test, latency was recorded as “30 minutes” for the purpose of data analysis, and mice were then returned to their home cage.

The **two-plate temperature preference assay** was performed as described previously (Minett et al., 2012). Two temperature-controlled metal plates were abutted together within a plexiglass enclosure. Mice were given the choice to travel between a probe temperature plate and a control temperature (always 30°C) plate for 10 minutes and the time spent per plate, distance traveled per plate and transitions between plates were recorded via a video camera above the enclosure (included with apparatus) and analyzed automatically via the accompanying software. Mice were tested twice for each probe temperature, and data for time/distance/transitions were represented as the average of both trials. In order to prevent mice from associating one plate as the control plate, the control plate was switched for each trial. Moreover, between testing for different probe temperatures, the initial position of the control plate was switched with the probe plate to prevent mice from associating the order of trials with the location of the control plate. As well, to encourage mice to sample both plates, mice were placed randomly on either the control plate or the probe plate for the first trial, and this order was then switched for the second trial.

The **hot-plate test** was performed as described previously (Mogil et al., 1999), and the cold-plate test was performed using similar methods. Mice were placed within the hot-cold plate apparatus (IITC PE34) on a stainless-steel metal plate heated to $53 \pm 0.1^\circ\text{C}$ or cooled to $0 \pm 0.1^\circ\text{C}$ and were video-recorded from the side (with a mirror opposite the test chamber to view each side of the mouse) for 60 s at which point they were returned to their home cage. The latency to either lick the hind paw, flutter of the hind paw or to attempt to escape via jumping was recorded. Additional behaviors were recorded: total time spent licking either hind paw, total hind paw licking episodes, total jumps and total hind paw flutters. Mice were tested once, and data were represented directly based on behaviors recorded in one 60 s trial. Entirely different cohorts of mice were used for the hot and cold-plate tests respectively, to prevent behavioral adaptation to the test.

The **acetone test** was performed as described previously (Colburn et al., 2007). Briefly, the mouse's hind paw was stimulated with a drop of acetone extruded from the blunt end of a 1ml syringe. Mice were recorded for 60 s following the application, and total time spent licking was recorded as well as the magnitude of behavior on a 0–2 scale as reported previously (Colburn et al., 2007). Mice were stimulated 5 times, with an inter-trial interval of at least 5 minutes. Total licking time was reported as a sum of 5 trials, and the behavioral score (0–2) was reported as an average of 5 trials.

The **foot clip test** was performed as described previously (Pan et al., 2019). Briefly, a toothless mechanical clip was used to pinch skin on the plantar surface of the hind paw, and mice were placed in a plexiglass cylinder (dimensions) on the glass sheet used previously and video recorded from below for 60 s (this recording setup is identical to the following formalin and capsaicin tests). The total amount of time licking the clipped hind paw was recorded, and data is presented as the total time licking during the one trial.

The **capsaicin and formalin tests** (Mogil et al., 1999; Sakurada et al., 1992) were performed similarly – mice were injected with approximately 20 μ L of capsaicin solution (1.5 μ g/20 μ L in 1 \times PBS) or formalin solution (2% in 1 \times PBS) in the plantar surface of the right hind paw using a standard 28G insulin syringe (BD) and video recorded from below for either 15 or 60 minutes respectively. Mice were tested only once on each test, with different cohorts of mice used for each respective test. Data were represented as time spent licking the injected hind paw. For formalin-injected animals, these data were analyzed separately acutely after injection (0–10 minutes) or chronically after injection (11–60 minutes).

Tissue fixation, freezing and sectioning—Adult mice were first anesthetised with a 0.3 mL i.p injection of Ketamine/Xylazine solution (10 mg/ml Ketamine, 1 mg/ml Xylazine, in 0.9% saline). Transcardial perfusion was done with a peristaltic pump (Gilson miniPuls2). Mice were perfused with 10 mL of ice cold 1 \times PBS followed by 20 mL of ice cold 4% PFA in 1 \times PBS. Brains and spinal cords were dissected and post-fixed in 4% PFA in 1 \times PBS at 4°C for two hours, washed briefly in 1 \times PBS, and acclimated to 30% sucrose for 1–2 days or until sunk. After cryoprotection, tissue was frozen in OCT Compound and cryosectioned at –22°C. Tissue was cut into 25 μ m sections for all experiments other than RNA Scope, in which case 10 μ m sections were used, and those involving *Ptf1a*^{CRE} and *Ascl1*^{GFP} lines where 30 μ m sections were used.

Immunohistochemistry—For mouse tissue, sections were heated at 37°C for 15 minutes prior to immunohistochemistry. Following this, sections were washed three times in 1 \times PBS for 10 minutes, blocked using a solution of 5% heat-inactivated horse serum (HIHS) and 0.1% Triton X-100 in 1 \times PBS (0.1% tPBS) for 30 minutes, and incubated with a primary antibody solution (in 1% HIHS, 0.1% tPBS) overnight at 4°C. The following day, sections were again washed three times in 1 \times PBS for 10 minutes, and incubated with a secondary antibody solution (in 1% HIHS, 0.1% tPBS) at room temperature for 1 hour. Following this, sections were washed three more times in 1 \times PBS for 10 minutes and coverslipped using a Mowiol solution (10% Mowiol - Sigma, 25% glycerol). Slides were allowed to dry in the dark at room temperature and subsequently imaged using fluorescent microscopy. For

immunohistochemistry involving the anti-BrdU antibody, two rounds of immunohistochemistry were done: the first round involved staining for RFP or Phox2a and the second round for BrdU with some modifications. Prior to the anti-BrdU primary antibody incubation, slides were treated in a 2 N hydrochloric acid solution at 37°C for 30 minutes. Subsequently, slides were neutralized by washing in a Tris-buffered saline solution (pH 8.5, 50 mM Tris, 150 mM NaCl) for 10 minutes at room temperature, after which primary antibody incubation was done. BrdU immunohistochemistry proceeded in two steps, as acid denaturation of DNA reveals anti-BrdU epitopes but destroys RFP/Phox2a epitopes; however, acid denaturation does not destroy secondary antibody-conjugated fluorophores from the first round of immunohistochemistry. Immunohistochemistry on human tissue was performed on cryostat sections after blocking in 0.2% gelatin in PBS containing 0.25% Triton X-100 (Sigma). Sections were then incubated overnight with respective primary antibodies, all used at 1:500 dilutions, followed by 2 hours incubation in appropriate secondary antibodies. In figures demonstrating tdT signal, amplification was done using an anti-RFP antibody (see key resources table).

In situ-hybridization (ISH)—ISH was done using RNA Scope® Multiplex Fluorescent v2 kits, according to manufacturer's instructions. All experiments used Mm-Phox2a-C2 coupled to Opal™ 520, Mm-Lmx1b-C3 coupled to Opal™ 690, and all other candidate probes being compared to Phox2a (all Mm C1 probes) were coupled to Opal™ 570.

In-ovo chicken electroporation and tissue processing—Fertilized White Leghorn eggs were obtained from the Texas A&M Poultry Department (College Station, TX, USA) and incubated for 48 hours at 39°C. The supercoiled reporter plasmid *ePhox2a-GFP* was diluted to 1.5 mg/mL in H₂O/1X loading dye and injected into the lumen of the closed neural tube at stages Hamburger-Hamilton (HH) stages 13–15 (~E2) along with either a *pMiVIII-Myc* epitope tagged plasmid serving as an electroporation control or the same plasmid containing the coding region of *Ascl1*, *Ptf1a*, or *Prdm13* (Hamburger and Hamilton, 1951). The injected embryos were then electroporated with 5 pulses of 25 mV each for 50 msec with intervals of 100 msec. Embryos were harvested 48 hours later at HH stages 22–23 (~E4), fixed with 4% paraformaldehyde for 45 minutes, and processed for cryosectioning and immunofluorescence.

Generation of reporter constructs and expression vectors—Previously published ChIP-seq data for *Ascl1*, *Ptf1a*, *Rbpj*, and *Prdm13* (Borromeo et al., 2014; Meredith et al., 2013; Mona et al., 2017) (GSE55840; GSE90938) were used to identify a putative enhancer for *Phox2a* in the chicken dorsal neural tube. An 851 bp region (chr7:101834344–101835194 from mm10) encompassing two peaks bound by *Ascl1* and *Ptf1a* was cloned into the MCSIII GFP reporter cassette (*ePhox2a-GFP*). This reporter cassette contains the β -globin minimal promoter, a nuclear localized fluorescence reporter, and the 3' cassette from the human growth hormone. The *ePhox2a* sequence was PCR amplified from ICR mouse DNA. *Prdm13*, *mycPtf1a*, and *mycAscl1* were expressed in the pMiVIII expression vector (Chang et al., 2013; Gowan et al., 2001; Matsunaga et al., 2001). All constructs were sequence-verified and expression of the transcription factor confirmed by immunohistochemistry with antibodies to the myc tag or with factor-specific antibodies.

Epifluorescence and Confocal Microscopy—Micrographs of tissue sections were taken either with epifluorescence microscopes (Leica DM6, DM6000) or confocal microscopes (Leica SP8 or Zeiss LSM710). All RNA Scope images, for quantification and for analysis, were taken using confocal microscopes on a 40× objective in order to resolve single puncta.

Human sections were imaged with a laser scanning confocal microscope (FV1000, Olympus) and processed using ImageJ (NIH) and Adobe Photoshop.

QUANTIFICATION AND STATISTICAL ANALYSIS

Bioinformatics—scRNA-seq data used in this study were previously published (Delile et al., 2019), using spinal cord cells from E9.5, E10.5, E11.5, E12.5 and E13.5 mouse embryos and processed via the 10× Genomics Chromium Single Cell 3' v2 protocol. Raw data were extracted from ArrayExpress E-MTAB-7320). CellRanger v 2.1.1 (Zheng et al., 2017) was used to align reads to the 10X mm10 mouse reference genome v2.1.0, filter barcodes and quantify genes. Biological replicates from the same time points were then merged using CellRanger's *aggregate* function. All downstream analyses were performed on these 41 009 cells, using the Seurat v.3.1.1. R package.

Using Delile et al. (2019) annotation, only cells classified as neurons were kept for further analysis (18 048 cells). From these, data for each time point was normalized and highly variable genes identified using SCTransform's normalization and variance stabilizing methods (Hafemeister and Satija, 2019). Different time points were then integrated using CCA (Stuart et al., 2019). From the integrated dataset, 2 subsets were created: 1) all cells expressing *Lmx1b* (*Lmx1b*+) were isolated (2614 cells) and 2) all early (E9.5, E10.5 and E11.5) *Lmx1b* cells (186 cells). For each of these subsets, dimensionality reduction (PCA and UMAP) was applied and clusters identified using Seurat's SNN modularity optimization-based clustering Louvain algorithm. Differential expression analysis was performed on the non-integrated assay to identify markers for each cluster (Wilcoxon Rank Sum test).

A differential expression analysis was then performed on clusters of interest in each of these 3 subsets (cluster 6 from *Lmx1b* cells and clusters 2 and 3 in early *Lmx1b* cells). Each of these clusters was compared to all other neuron cells in order to identify specific markers within these clusters. This analysis was limited to genes which had on average, at least 0.1 log-Fold difference between the two groups compared and present in at least 10% of cells of either group. Markers were then considered significantly differentially expressed if adjusted p values < 0.05.

Cell counts—All cell counts were done with ImageJ v. 2.0.0 software, using the cell counter plugin. Data was recorded and sorted in Microsoft Excel.

Animal Behavior—Video-recordings of mice were quantified by R.B.R and M.B using Aegisub (free subtitling software), which includes video annotation functions allowing precise start and stop times for specified behaviors to be recorded. Data was exported and then sorted in Microsoft Excel.

Data representation—Graphs display data points from individual animals (hollow circles), mean data from all animals (bars), and \pm standard error of the mean (error bars).

Numbers—All numbers are noted in figure legends. In all experiments using adult mice, n represents unique individuals. In all experiments using embryonic mice, n represents unique embryos. No data represented as single ns have been pooled from multiple individual animals.

Statistics—All statistical analyses were performed using GraphPad Prism v8.3.0 software, except those involving single cell RNA-Seq data processing, which are described in Bioinformatics (above). Statistical tests used are described in figure legends. Significance is represented as ns: non significant, * $p < 0.05$, ** $p < 0.01$ or *** $p < 0.001$.

Supplementary Material

Refer to Web version on PubMed Central for supplementary material.

ACKNOWLEDGMENTS

We thank Meirong Liang, Julie Cardin, Qinzhang Zhu, and Colleen Barrick for technical assistance; Laura Kus (GENSAT) for advice on transgenic mouse design; Caroline Grou and Virginie Calderon for bioinformatics analyses; J.-F. Brunet for the Phox2a and Phox2b antiserum and advice; Carmen Birchmeier for Lmx1b, Tlx3, and Lbx1 antisera; Jay Bikoff for the Pou6F2 antiserum; Laskaro Zagoraoui for Shox2 antiserum; Hanns Ulrich Zeilhofer for the *Hoxb8^{Cre}* mice; Jeff Mogil, Yves de Koninck, and Stefano Stifani for discussions; and Jean-François Brunet, Adam Hantman, Denis Jabaudon, Jeff Mogil, Michel Cayouette, Sonia Paixao, Samuel Ferland, and Feng Wang for comments on the manuscript.

R.B.R. was a recipient of a PhD studentship from Fonds de Recherche du Québec - Santé. S.R.-P. received a studentship from McGill University's Healthy Brains, Healthy Lives (HBHL) initiative supported, in part, by the Canada First Research Excellence Fund. J.E.J. was supported by the National Institutes of Health grant R37 HD091856. A.C. was supported by the Agence Nationale de la Recherche and Inserm (transversal program HuDeCa). L.T. was supported by the Intramural Research Program of NCI, NIH. A.K. and M.K. were funded by operating and project grants from the Canadian Institutes of Health Research (PJT-162225, MOP-77556, PJT-153053, and PJT-159839 to A.K. and MOP-127110 and PJT-162143 to M.K.).

REFERENCES

- Allen Institute for Brain Science (2004). Allen Mouse Brain Atlas <https://mouse.brain-map.org/static/atlas>.
- Allen Institute for Brain Science (2008). Allen Spinal Cord Atlas <http://mousespinal.brain-map.org/>.
- Altman J, and Bayer SA (2001). Development of the Human Spinal Cord: An Interpretation Based on Experimental Studies in Animals (Oxford University Press).
- Andrew D, and Craig AD (2001). Spinothalamic lamina I neurons selectively sensitive to histamine: a central neural pathway for itch. *Nat. Neurosci* 4, 72–77. [PubMed: 11135647]
- Apkarian AV, Stevens RT, and Hodge CJ (1985). Funicular location of ascending axons of lamina I cells in the cat spinal cord. *Brain Res* 334, 160–164. [PubMed: 3995308]
- Arber S (2012). Motor circuits in action: specification, connectivity, and function. *Neuron* 74, 975–989. [PubMed: 22726829]
- Bernard JF, Dallel R, Raboisson P, Villanueva L, and Le Bars D (1995). Organization of the efferent projections from the spinal cervical enlargement to the parabrachial area and periaqueductal gray: a PHA-L study in the rat. *J. Comp. Neurol* 353, 480–505. [PubMed: 7759612]
- Berthier M, Starkstein S, and Leiguarda R (1988). Asymbolia for pain: a sensory-limbic disconnection syndrome. *Ann. Neurol* 24, 41–49. [PubMed: 3415199]

- Borromeo MD, Meredith DM, Castro DS, Chang JC, Tung KC, Guillemot F, and Johnson JE (2014). A transcription factor network specifying inhibitory versus excitatory neurons in the dorsal spinal cord. *Development* 141, 2803–2812. [PubMed: 24924197]
- Bouet V, Boulouard M, Toutain J, Divoux D, Bernaudin M, Schumann-Bard P, and Freret T (2009). The adhesive removal test: a sensitive method to assess sensorimotor deficits in mice. *Nat. Protoc* 4, 1560–1564. [PubMed: 19798088]
- Bourgeois L, Monconduit L, Villanueva L, and Bernard JF (2001). Parabrachial internal lateral neurons convey nociceptive messages from the deep laminae of the dorsal horn to the intralaminar thalamus. *J. Neurosci* 21, 2159–2165. [PubMed: 11245700]
- Bourojeni FB, Zeilhofer HU, and Kania A (2020). Netrin1 receptor DCC is required for the contralateral topography of lamina I anterolateral system neurons. *Pain*, Published July 21, 2020. 10.1097/j.pain.0000000000002012.
- Britz O, Zhang J, Grossmann KS, Dyck J, Kim JC, Dymecki S, Gosgnach S, and Goulding M (2015). A genetically defined asymmetry underlies the inhibitory control of flexor-extensor locomotor movements. *eLife* 4, 04718.
- Brunet JF, and Pattyn A (2002). Phox2 genes - from patterning to connectivity. *Curr. Opin. Genet. Dev* 12, 435–440. [PubMed: 12100889]
- Cameron D, Polgár E, Gutierrez-Mecinas M, Gomez-Lima M, Watanabe M, and Todd AJ (2015). The organisation of spinoparabrachial neurons in the mouse. *Pain* 156, 2061–2071. [PubMed: 26101837]
- Chang JC, Meredith DM, Mayer PR, Borromeo MD, Lai HC, Ou YH, and Johnson JE (2013). Prdm13 mediates the balance of inhibitory and excitatory neurons in somatosensory circuits. *Dev. Cell* 25, 182–195. [PubMed: 23639443]
- Chaplan SR, Bach FW, Pogrel JW, Chung JM, and Yaksh TL (1994). Quantitative assessment of tactile allodynia in the rat paw. *J. Neurosci. Methods* 53, 55–63. [PubMed: 7990513]
- Colburn RW, Lubin ML, Stone DJ Jr., Wang Y, Lawrence D, D'Andrea MR, Brandt MR, Liu Y, Flores CM, and Qin N (2007). Attenuated cold sensitivity in TRPM8 null mice. *Neuron* 54, 379–386. [PubMed: 17481392]
- Craig AD (2003a). A new view of pain as a homeostatic emotion. *Trends Neurosci* 26, 303–307. [PubMed: 12798599]
- Craig AD (2003b). Pain mechanisms: labeled lines versus convergence in central processing. *Annu. Rev. Neurosci* 26, 1–30. [PubMed: 12651967]
- Craig AD (2004). Lamina I, but not lamina V, spinothalamic neurons exhibit responses that correspond with burning pain. *J. Neurophysiol* 92, 2604–2609. [PubMed: 15163673]
- Craig AD, and Serrano LP (1994). Effects of systemic morphine on lamina I spinothalamic tract neurons in the cat. *Brain Res* 636, 233–244. [PubMed: 8012807]
- Davidson S, Truong H, and Giesler GJ Jr. (2010). Quantitative analysis of spinothalamic tract neurons in adult and developing mouse. *J. Comp. Neurol* 518, 3193–3204. [PubMed: 20575056]
- Delile J, Rayon T, Melchionda M, Edwards A, Briscoe J, and Sagner A (2019). Single cell transcriptomics reveals spatial and temporal dynamics of gene expression in the developing mouse spinal cord. *Development* 146, dev173807. [PubMed: 30846445]
- Deng J, Zhou H, Lin JK, Shen ZX, Chen WZ, Wang LH, Li Q, Mu D, Wei YC, Xu XH, and Sun YG (2020). The Parabrachial Nucleus Directly Channels Spinal Nociceptive Signals to the Intralaminar Thalamic Nuclei, but Not the Amygdala. *Neuron* 107, 909–923.e6. [PubMed: 32649865]
- Ding YQ, Yin J, Kania A, Zhao ZQ, Johnson RL, and Chen ZF (2004). Lmx1b controls the differentiation and migration of the superficial dorsal horn neurons of the spinal cord. *Development* 131, 3693–3703. [PubMed: 15229182]
- Ding YQ, Kim JY, Xu YS, Rao Y, and Chen ZF (2005). Ventral migration of early-born neurons requires Dcc and is essential for the projections of primary afferents in the spinal cord. *Development* 132, 2047–2056. [PubMed: 15788454]
- Dong HW (2008). *The Allen Reference Atlas: A Digital Color Brain Atlas of the C57BL/6J Male Mouse* (John Wiley & Sons).

- Dougherty KJ, Zagoraoui L, Satoh D, Rozani I, Doobar S, Arber S, Jessell TM, and Kiehn O (2013). Locomotor rhythm generation linked to the output of spinal shox2 excitatory interneurons. *Neuron* 80, 920–933. [PubMed: 24267650]
- Duan B, Cheng L, Bourane S, Britz O, Padilla C, Garcia-Campmany L, Krashes M, Knowlton W, Velasquez T, Ren X, et al. (2014). Identification of spinal circuits transmitting and gating mechanical pain. *Cell* 159, 1417–1432. [PubMed: 25467445]
- Fan Y, Chen P, Raza MU, Szebeni A, Szebeni K, Ordway GA, Stockmeier CA, and Zhu MY (2018). Altered Expression of Phox2 Transcription Factors in the Locus Coeruleus in Major Depressive Disorder Mimicked by Chronic Stress and Corticosterone Treatment In Vivo and In Vitro. *Neuroscience* 393, 123–137. [PubMed: 30315878]
- Feil K, and Herbert H (1995). Topographic organization of spinal and trigeminal somatosensory pathways to the rat parabrachial and Kölliker-Fuse nuclei. *J. Comp. Neurol* 353, 506–528. [PubMed: 7759613]
- Freeman W, and Watts JW (1948). Pain mechanisms and the frontal lobes; a study of prefrontal lobotomy for intractable pain. *Ann. Intern. Med* 28, 747–754. [PubMed: 18911006]
- Gauriau C, and Bernard JF (2004). A comparative reappraisal of projections from the superficial laminae of the dorsal horn in the rat: the forebrain. *J. Comp. Neurol* 468, 24–56. [PubMed: 14648689]
- GENSAT (2008). The Gene Expression Nervous System Atlas (GENSAT) Project, NINDS Contracts N01NS02331 & HHSN271200723701C to The Rockefeller University (New York, NY). <http://www.gensat.org/GeneProgressTracker.jsp?gensatGeneID=1715>.
- Glasgow SM, Henke RM, Macdonald RJ, Wright CV, and Johnson JE (2005). Ptf1a determines GABAergic over glutamatergic neuronal cell fate in the spinal cord dorsal horn. *Development* 132, 5461–5469. [PubMed: 16291784]
- Goulding M (2009). Circuits controlling vertebrate locomotion: moving in a new direction. *Nat. Rev. Neurosci* 10, 507–518. [PubMed: 19543221]
- Gowan K, Helms AW, Hunsaker TL, Collisson T, Ebert PJ, Odom R, and Johnson JE (2001). Crossinhibitory activities of Ngn1 and Math1 allow specification of distinct dorsal interneurons. *Neuron* 31, 219–232. [PubMed: 11502254]
- Guilbaud G, Peschanski M, Gautron M, and Binder D (1980). Neurones responding to noxious stimulation in VB complex and caudal adjacent regions in the thalamus of the rat. *Pain* 8, 303–318. [PubMed: 7402691]
- Hafemeister C, and Satija R (2019). Normalization and variance stabilization of single-cell RNA-seq data using regularized negative binomial regression. *Genome Biol* 20, 296. [PubMed: 31870423]
- Hamburger V, and Hamilton HL (1951). A series of normal stages in the development of the chick embryo. *J. Morphol* 88, 49–92. [PubMed: 24539719]
- Han S, Soleiman MT, Soden ME, Zweifel LS, and Palmiter RD (2015). Elucidating an Affective Pain Circuit that Creates a Threat Memory. *Cell* 162, 363–374. [PubMed: 26186190]
- Hargreaves K, Dubner R, Brown F, Flores C, and Joris J (1988). A new and sensitive method for measuring thermal nociception in cutaneous hyperalgesia. *Pain* 32, 77–88. [PubMed: 3340425]
- Helms AW, Battiste J, Henke RM, Nakada Y, Simplicio N, Guillemot F, and Johnson JE (2005). Sequential roles for Mash1 and Ngn2 in the generation of dorsal spinal cord interneurons. *Development* 132, 2709–2719. [PubMed: 15901662]
- Hori K, Cholewa-Waclaw J, Nakada Y, Glasgow SM, Masui T, Henke RM, Wildner H, Martarelli B, Beres TM, Epstein JA, et al. (2008). A nonclassical bHLH Rbpj transcription factor complex is required for specification of GABAergic neurons independent of Notch signaling. *Genes Dev* 22, 166–178. [PubMed: 18198335]
- Huang T, Lin SH, Malewicz NM, Zhang Y, Zhang Y, Goulding M, La-Motte RH, and Ma Q (2019). Identifying the pathways required for coping behaviours associated with sustained pain. *Nature* 565, 86–90. [PubMed: 30532001]
- Hyndman OR, and Jarvis FJ (1940). Gastric crisis of tabes dorsalis: Treatment by anterior chordotomy in eight cases. *Arch. Surg* 40, 997–1013.
- Hyndman OR, and Wolkin J (1943). Anterior chordotomy: Further observations on physiologic results and optimum manner of performance. *Arch. Neurol. Psychiatry* 50, 129–148.

- Kawaguchi Y, Cooper B, Gannon M, Ray M, MacDonald RJ, and Wright CV (2002). The role of the transcriptional regulator Ptf1a in converting intestinal to pancreatic progenitors. *Nat. Genet* 32, 128–134. [PubMed: 12185368]
- Kim EJ, Battiste J, Nakagawa Y, and Johnson JE (2008). Ascl1 (Mash1) lineage cells contribute to discrete cell populations in CNS architecture. *Mol. Cell. Neurosci* 38, 595–606. [PubMed: 18585058]
- Kitamura T, Yamada J, Sato H, and Yamashita K (1993). Cells of origin of the spinoparabrachial fibers in the rat: a study with fast blue and WGA-HRP. *J. Comp. Neurol* 328, 449–461. [PubMed: 8440790]
- Kohwi M, and Doe CQ (2013). Temporal fate specification and neural progenitor competence during development. *Nat. Rev. Neurosci* 14, 823–838. [PubMed: 24400340]
- Lai HC, Seal RP, and Johnson JE (2016). Making sense out of spinal cord somatosensory development. *Development* 143, 3434–3448. [PubMed: 27702783]
- Leah J, Men  tre  y D, and de Pommery J (1988). neuropeptides in long ascending spinal tract cells in the rat: evidence for parallel processing of ascending information. *Neuroscience* 24, 195–207. [PubMed: 3368049]
- Leung CT, Coulombe PA, and Reed RR (2007). Contribution of olfactory neural stem cells to tissue maintenance and regeneration. *Nat. Neurosci* 10, 720–726. [PubMed: 17468753]
- Liebl DJ, Klesse LJ, Tessarollo L, Wohlman T, and Parada LF (2000). Loss of brain-derived neurotrophic factor-dependent neural crest-derived sensory neurons in neurotrophin-4 mutant mice. *Proc. Natl. Acad. Sci. USA* 97, 2297–2302. [PubMed: 10681461]
- Mantyh PW, Rogers SD, Honore P, Allen BJ, Ghilardi JR, Li J, Daughters RS, Lappi DA, Wiley RG, and Simone DA (1997). Inhibition of hyperalgesia by ablation of lamina I spinal neurons expressing the substance P receptor. *Science* 278, 275–279. [PubMed: 9323204]
- Marklund U, Alekseenko Z, Andersson E, Falci S, Westgren M, Perlmann T, Graham A, Sundstr  m E, and Ericson J (2014). Detailed expression analysis of regulatory genes in the early developing human neural tube. *Stem Cells Dev* 23, 5–15. [PubMed: 24007338]
- Marshall GE, Shehab SA, Spike RC, and Todd AJ (1996). Neurokinin-1 receptors on lumbar spinothalamic neurons in the rat. *Neuroscience* 72, 255–263. [PubMed: 8730722]
- Masullo L, Mariotti L, Alexandre N, Freire-Pritchett P, Boulanger J, and Tripodi M (2019). Genetically Defined Functional Modules for Spatial Orienting in the Mouse Superior Colliculus. *Curr. Biol* 29, 2892–2904.e8. [PubMed: 31474533]
- Matsunaga E, Araki I, and Nakamura H (2001). Role of Pax3/7 in the tectum regionalization. *Development* 128, 4069–4077. [PubMed: 11641229]
- McMahon SB, and Wall PD (1983). A system of rat spinal cord lamina 1 cells projecting through the contralateral dorsolateral funiculus. *J. Comp. Neurol* 214, 217–223. [PubMed: 6841684]
- Melzack R, and Casey KL (1968). Sensory, motivational, and central control determinants of pain: A new conceptual model In *The Skin Senses*, Kenshalo DR, ed. (Charles C Thomas), pp. 423–439.
- Meredith DM, Borromeo MD, Deering TG, Casey BH, Savage TK, Mayer PR, Hoang C, Tung KC, Kumar M, Shen C, et al. (2013). Program specificity for Ptf1a in pancreas versus neural tube development correlates with distinct collaborating cofactors and chromatin accessibility. *Mol. Cell. Biol* 33, 3166–3179. [PubMed: 23754747]
- Minett MS, Nassar MA, Clark AK, Passmore G, Dickenson AH, Wang F, Malcangio M, and Wood JN (2012). Distinct Nav1.7-dependent pain sensations require different sets of sensory and sympathetic neurons. *Nat. Commun* 3, 791. [PubMed: 22531176]
- Mogil JS, Wilson SG, Bon K, Lee SE, Chung K, Raber P, Pieper JO, Hain HS, Belknap JK, Hubert L, et al. (1999). Heritability of nociception I: responses of 11 inbred mouse strains on 12 measures of nociception. *Pain* 80, 67–82. [PubMed: 10204719]
- Mona B, Uruena A, Kolipara RK, Ma Z, Borromeo MD, Chang JC, and Johnson JE (2017). Repression by PRDM13 is critical for generating precision in neuronal identity. *eLife* 6, e25787. [PubMed: 28850031]
- Morin X, Cremer H, Hirsch MR, Kapur RP, Goridis C, and Brunet JF (1997). Defects in sensory and autonomic ganglia and absence of locus coeruleus in mice deficient for the homeobox gene Phox2a. *Neuron* 18, 411–423. [PubMed: 9115735]

- Nakano M, Yamada K, Fain J, Sener EC, Selleck CJ, Awad AH, Zwaan J, Mullaney PB, Bosley TM, and Engle EC (2001). Homozygous mutations in ARIX(PHOX2A) result in congenital fibrosis of the extraocular muscles type 2. *Nat. Genet* 29, 315–320. [PubMed: 11600883]
- Nishida K, and Ito S (2017). Developmental origin of long-range neurons in the superficial dorsal spinal cord. *Eur. J. Neurosci* 46, 2608–2619. [PubMed: 28977701]
- Normes HO, and Carry M (1978). Neurogenesis in spinal cord of mouse: an autoradiographic analysis. *Brain Res* 159, 1–6. [PubMed: 728790]
- Pan H, Fatima M, Li A, Lee H, Cai W, Horwitz L, Hor CC, Zaher N, Cin M, Slade H, et al. (2019). Identification of a Spinal Circuit for Mechanical and Persistent Spontaneous Itch. *Neuron* 103, 1135–1149.e6. [PubMed: 31324538]
- Pattyn A, Morin X, Cremer H, Goridis C, and Brunet JF (1997). Expression and interactions of the two closely related homeobox genes Phox2a and Phox2b during neurogenesis. *Development* 124, 4065–4075. [PubMed: 9374403]
- Petitjean H, Bourojeni FB, Tsao D, Davidova A, Sotocinal SG, Mogil JS, Kania A, and Sharif-Naeini R (2019). Recruitment of Spinoparabrachial Neurons by Dorsal Horn Calretinin Neurons. *Cell Rep* 28, 1429–1438.e4. [PubMed: 31390558]
- Ren K, and Dubner R (2009). Descending control mechanisms In *Science of Pain*, Basbaum AI and Bushnell C, eds. (Elsevier), pp. 723–749.
- Rubins JL, and Friedman ED (1948). Asymbolia for pain. *Arch. Neurol. Psychiatry* 60, 554–573.
- Sakurada T, Katsumata K, Tan-No K, Sakurada S, and Kisara K (1992). The capsaicin test in mice for evaluating tachykinin antagonists in the spinal cord. *Neuropharmacology* 31, 1279–1285. [PubMed: 1281912]
- Smeyne RJ, Klein R, Schnapp A, Long LK, Bryant S, Lewin A, Lira SA, and Barbacid M (1994). Severe sensory and sympathetic neuropathies in mice carrying a disrupted Trk/NGF receptor gene. *Nature* 368, 246–249. [PubMed: 8145823]
- Spiller WG, and Martin E (1912). The treatment of persistent pain of organic origin in the lower part of the body by division of the anterolateral column of the spinal cord. *J. Am. Med. Assoc* LVIII, 1489–1490.
- Stuart T, Butler A, Hoffman P, Hafemeister C, Papalexi E, Mauck WM 3rd, Hao Y, Stoeckius M, Smibert P, and Satija R (2019). Comprehensive Integration of Single-Cell Data. *Cell* 177, 1888–1902.e1821. [PubMed: 31178118]
- Szabo NE, da Silva RV, Sotocinal SG, Zeilhofer HU, Mogil JS, and Kania A (2015). Hoxb8 intersection defines a role for Lmx1b in excitatory dorsal horn neuron development, spinofugal connectivity, and nociception. *J. Neurosci* 35, 5233–5246. [PubMed: 25834049]
- Tiveron MC, Hirsch MR, and Brunet JF (1996). The expression pattern of the transcription factor Phox2 delineates synaptic pathways of the autonomic nervous system. *J. Neurosci* 16, 7649–7660. [PubMed: 8922421]
- Wang X, Babayan AH, Basbaum AI, and Phelps PE (2012). Loss of the Reelin-signaling pathway differentially disrupts heat, mechanical and chemical nociceptive processing. *Neuroscience* 226, 441–450. [PubMed: 22999972]
- Warming S, Costantino N, Court DL, Jenkins NA, and Copeland NG (2005). Simple and highly efficient BAC recombineering using galK selection. *Nucleic Acids Res* 33, e36. [PubMed: 15731329]
- Watanabe K, Tamamaki N, Furuta T, Ackerman SL, Ikenaka K, and Ono K (2006). Dorsally derived netrin 1 provides an inhibitory cue and elaborates the ‘waiting period’ for primary sensory axons in the developing spinal cord. *Development* 133, 1379–1387. [PubMed: 16510500]
- Watanabe S, Sanuki R, Sugita Y, Imai W, Yamazaki R, Kozuka T, Ohsuga M, and Furukawa T (2015). Prdm13 regulates subtype specification of retinal amacrine interneurons and modulates visual sensitivity. *J. Neurosci* 35, 8004–8020. [PubMed: 25995483]
- Willis WD, Trevino DL, Coulter JD, and Maunz RA (1974). Responses of primate spinothalamic tract neurons to natural stimulation of hindlimb. *J. Neurophysiol* 37, 358–372. [PubMed: 4205568]
- Willis WD, Kenshalo DR Jr., and Leonard RB (1979). The cells of origin of the primate spinothalamic tract. *J. Comp. Neurol* 188, 543–573. [PubMed: 118192]

- Witschi R, Johansson T, Morscher G, Scheurer L, Deschamps J, and Zeilhofer HU (2010). Hoxb8-Cre mice: A tool for brain-sparing conditional gene deletion. *Genesis* 48, 596–602. [PubMed: 20658520]
- Yvone GM, Zhao-Fleming HH, Udeochu JC, Chavez-Martinez CL, Wang A, Hirose-Ikeda M, and Phelps PE (2017). Disabled-1 dorsal horn spinal cord neurons co-express Lmx1b and function in nociceptive circuits. *Eur. J. Neurosci* 45, 733–747. [PubMed: 28083884]
- Zheng GX, Terry JM, Belgrader P, Ryvkin P, Bent ZW, Wilson R, Ziraldo SB, Wheeler TD, McDermott GP, Zhu J, et al. (2017). Massively parallel digital transcriptional profiling of single cells. *Nat. Commun* 8, 14049. [PubMed: 28091601]

Highlights

- Phox2a is transiently expressed in embryonic anterolateral system (AS) spinal neurons
- Phox2a AS neuron development reflects AS neuron diversity
- Spinal *Phox2a* knockout causes aberrant AS connectivity and nociceptive defects
- Human and mouse embryonic spinal Phox2a neurons are similar

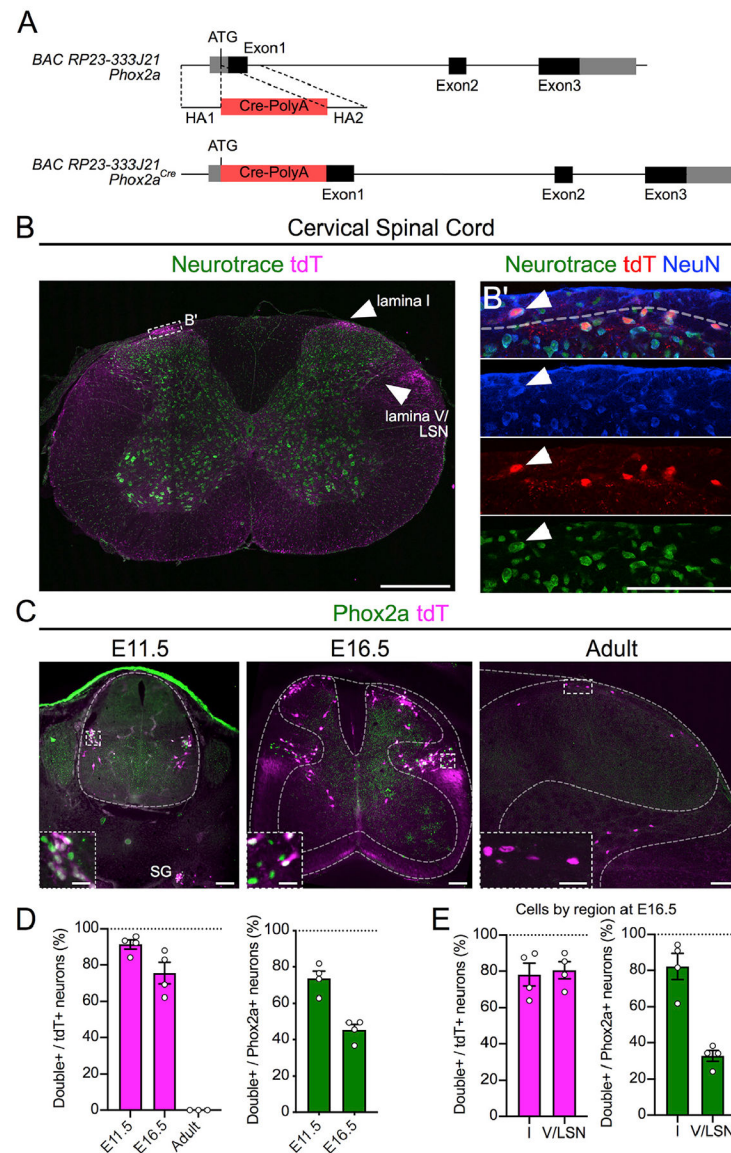


Figure 1. Spinal *Phox2a*^{Cre} Neurons Reside in Lamina I, Lamina V, and LSN All images are of *Phox2a*^{Cre}; *R26*^{LSL-tdT}/+ mice.

(A) BAC recombination strategy: *Cre-PolyA* insertion 3' to the *Phox2a* ATG codon in the BAC RP23-333J21.

(B) tdTomato (tdT)+ neurons in lamina I, lamina V, and LSN of the cervical spinal cord of adult mice.

(B') Magnified box in (B) showing lamina I Neurotrace, tdT, and NeuN co-labeling.

(C) Expression of tdT and *Phox2a* in E11.5, E16.5, and adult mouse spinal cord.

(D) Percentage of tdT+ neurons that express *Phox2a*, as well as percentage of *Phox2a*+ neurons that express tdT at E11.5 and E16.5 and in adult mice.

(E) Percentage of tdT+ neurons that express *Phox2a*, as well as percentage of *Phox2a*+ neurons that express tdT in the superficial and deep dorsal horn of E16.5 mouse spinal cords.

n = 4 E11.5 mice, n = 4 E16.5 mice, and n = 3 adult *Phox2a*^{Cre}; *R26*^{LSL-tdT}⁺ mice. Data are represented as mean ± SEM. Scale bars: 500 µm in (B), 100 µm in (B'), 100 µm in (C), and 25 µm in insets. SG, sympathetic ganglia.

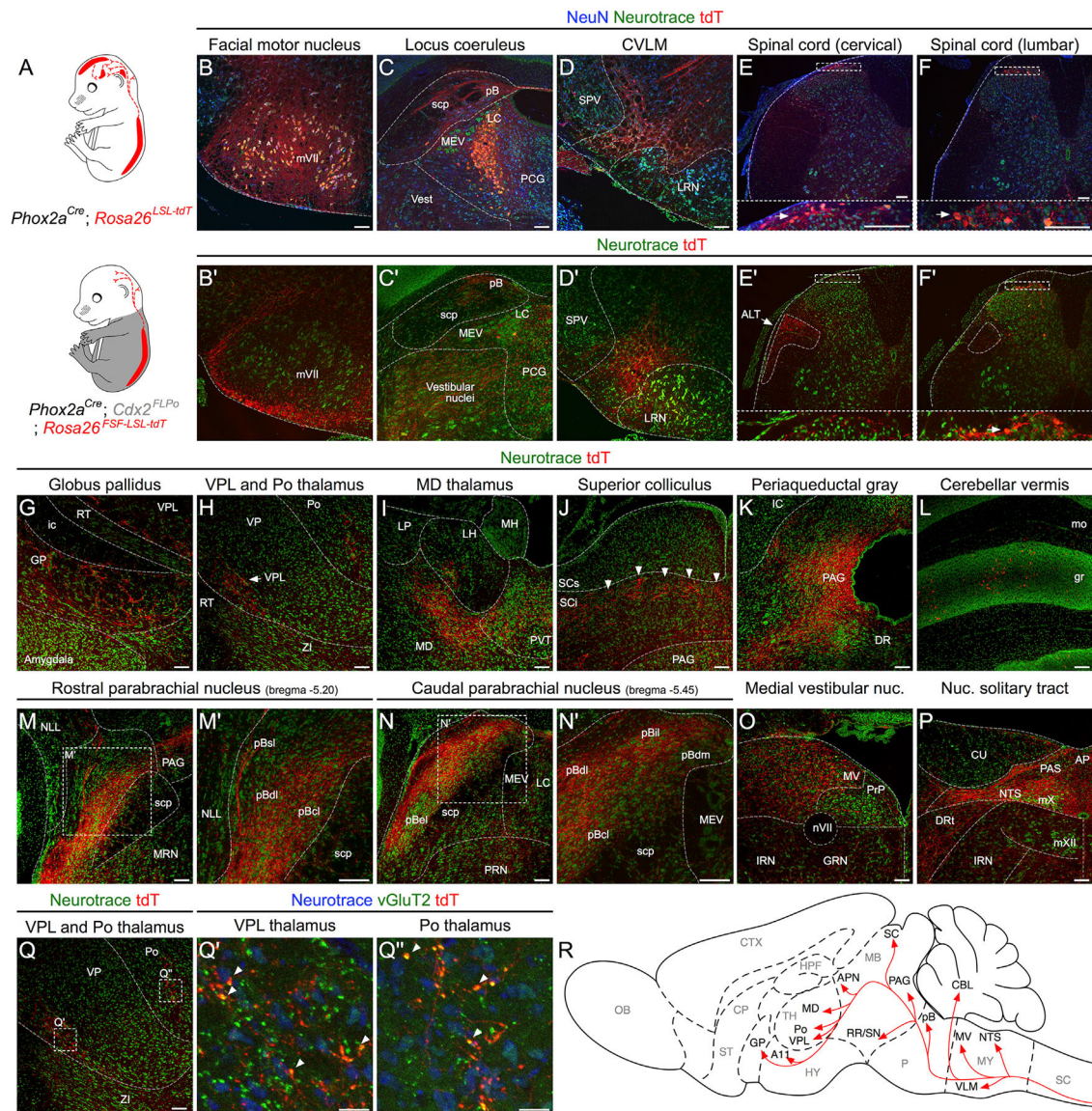


Figure 2. Spinal *Phox2a*^{Cre} Neurons Innervate AS Targets

(A) Intersectional genetic strategy to visualize spinofugal axons with tdT. *Phox2a*^{Cre}; *R26*^{LSL-tdT} mice have tdT cellular expression in the brain and spinal cord, while *Phox2a*^{Cre}; *Cdx2*^{FlpO}; *R26*^{FSF-LSL-tdT} mice have cellular tdT expression only in spinal *Phox2a* neurons.

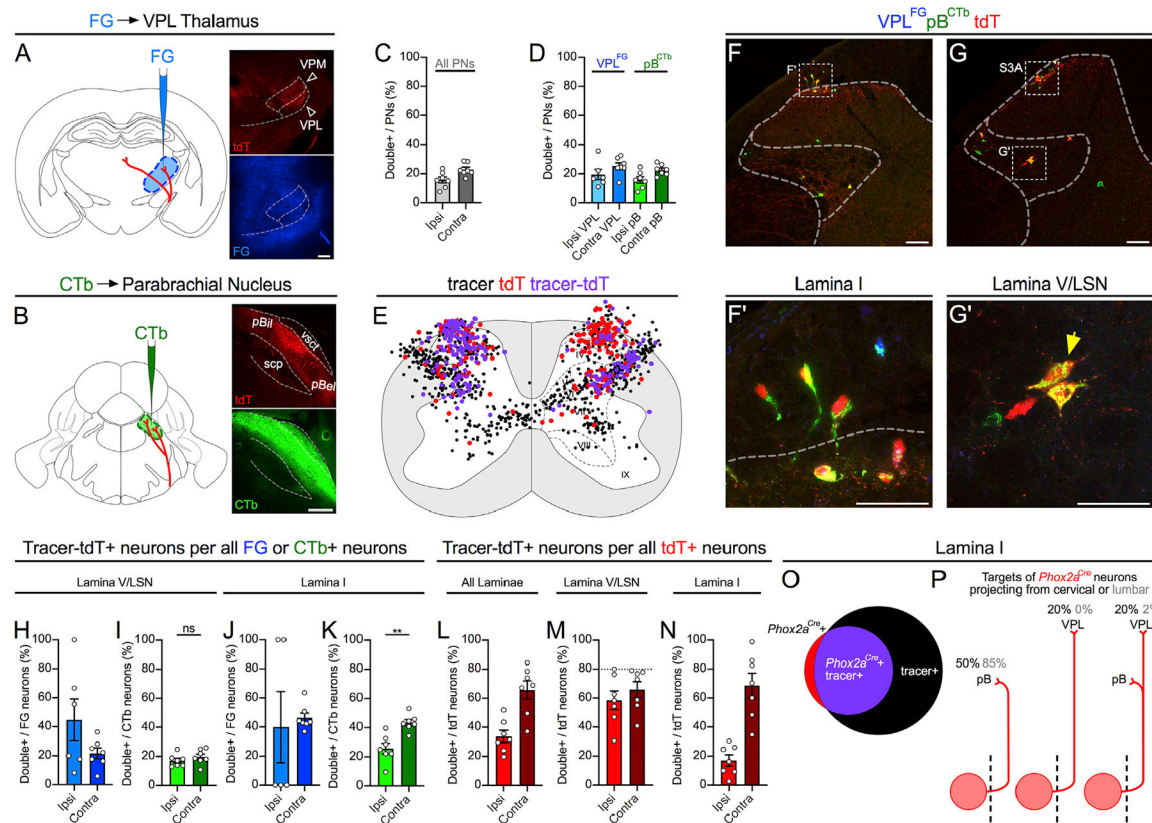
(B–F') In (B)–(F): expression of cellular tdT in the brain and spinal cord of *Phox2a*^{Cre}; *R26*^{LSL-tdT} mice in comparison to (B'–F') the lack of tdT expression in the brain and spinal cord of *Phox2a*^{Cre}; *Cdx2*^{FlpO}; *R26*^{FSF-LSL-tdT} mice, except caudal to the cervical level. In (E'), arrow indicates presumptive anterolateral tract (ALT) axons in white matter. Insets in (E), (F), (E'), and (F') correspond to stippled boxes and show tdT+ cell bodies (white arrows)

(G–P) Prominent targets of tdT+ spinofugal axons. Higher magnifications are shown in (M') and (N').

(Q–Q'') vGluT2 and tdT immunohistochemistry in the thalamus demonstrates putative excitatory synaptic termini arising from spinofugal axons. The image in (Q) is duplicated from (H) and is used as a reference for (Q') and (Q'').

(R) Diagram summarizing the termination sites of tdT+ spinofugal axons.

n = 3 *Phox2a*^{Cre}; *R26*^{LSL-tdT} adult mice, and n = 3 *Phox2a*^{Cre}; *Cdx2*^{FloP0}; *R26*^{FSF-LSL-tdT} adult mice. Scale bars: 100 μm, except 25 μm for (Q') and (Q''). AP, area postrema; CU, cuneate nucleus; DR, dorsal raphe; DRt, dorsal reticular nucleus; GRN, gigantocellular reticular nucleus; ic, internal capsule; IRN, intermediate reticular nucleus; LH, lateral habenula; LP, lateral posterior thalamus; LRN, lateral reticular nucleus; MEV, midbrain trigeminal nucleus; MH, medial habenula; mo, molecular layer of the cerebellum; MV, medial vestibular nucleus; mVII, facial motor nucleus; mX, vagal motor nucleus; mXII, hypoglossal motor nucleus; NLL, nucleus of the lateral lemniscus; nVII, facial motor nerve; PAS, parasolitary nucleus; pBdm, dorsal-medial parabrachial nucleus; PCG, pontine central gray; PRN, pontine reticular nucleus; PRP, nucleus prepositus; PVT, paraventricular thalamus; RT, reticular thalamic nucleus; SCi, superior colliculus, intermediate laminae; scp, superior cerebellar peduncle; SCs, superior colliculus, superficial laminae; SPV, spinal trigeminal nucleus; ZI, zona incerta.



(P) Diagrams illustrating the estimated percentages of cervical and lumbar lamina I *Phox2a*^{Cre} neurons projecting to mouse pB, VPL, or both. Stippled line represents spinal midline.

n = 7 *Phox2a*^{Cre}; *R26^{LSL-tdT}*⁺ adult mice (4 male, 3 female). Mann-Whitney test in (I) and (K); **p < 0.01; ns, non-significant. Data are represented as mean ± SEM. Scale bars: 250 μm in (A) and (B), 100 μm in (F) and (G), and 50 μm in (F') and (G').

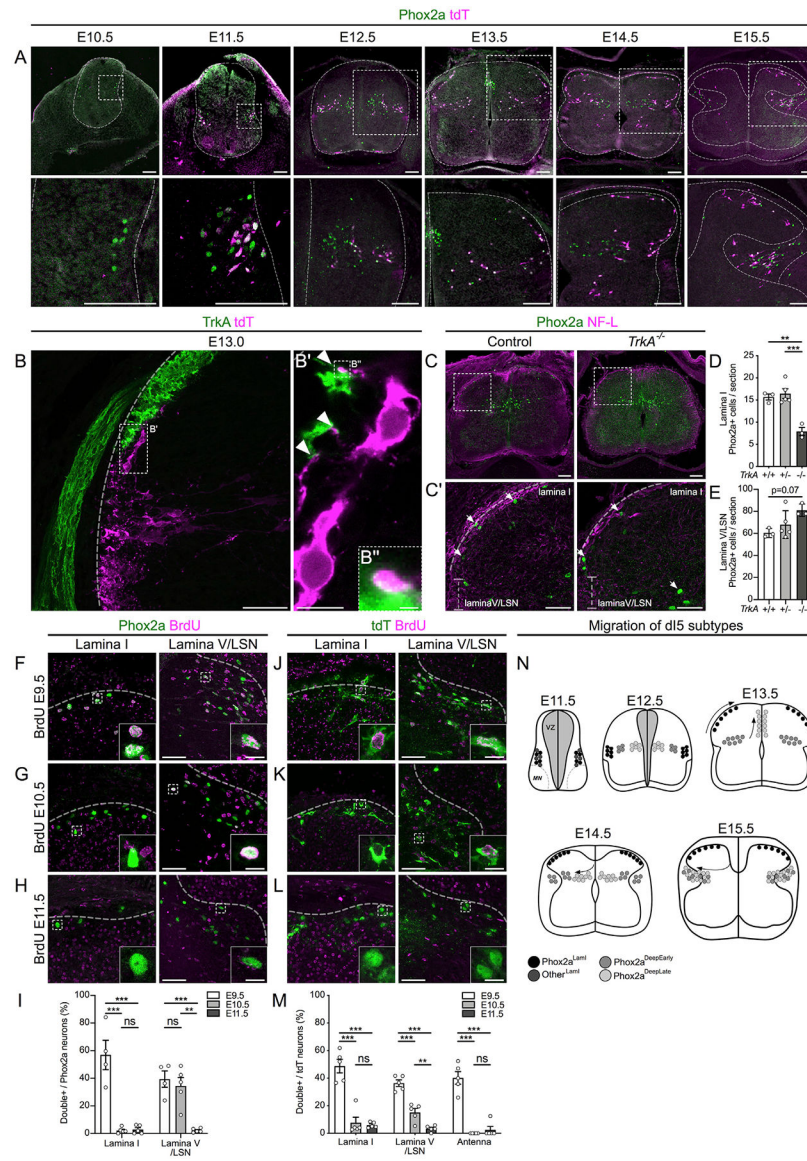


Figure 4. Heterogeneity of Spinal Phox2a Neuron Migration, Sensory Afferent Interaction, and Birth Time

(A) Migration of Phox2a⁺ and tdT⁺ neurons in embryonic spinal cords of *Phox2a^{Cre}; R26^{LSL-tdT}* mice between E10.5 and E15.5. Boxed regions in upper panels are magnified below.

(B–B'') Location of tdT⁺ neurons in the dorsal horn of *Phox2a^{Cre}; R26^{LSL-tdT}* spinal cords at E13.0, highlighting contacts (B' and B'') between lamina I neurons and TrkA⁺ sensory afferents (white arrowheads).

(C–E) Spinal Phox2a neuron (white arrows) location in E14.5 *TrkA^{+/+}*, *TrkA^{+/-}*, and *TrkA^{-/-}* mouse embryos. Boxed regions in (C) are magnified in (C').

(D and E) Counts of Phox2a neurons in lamina I (D) and lamina V/LSN (E).

(F–M) Birthdating of spinal Phox2a (F–I) or tdT (J–M) neurons in E16.5 *Phox2a^{Cre}; R26^{LSL-tdT}* mouse embryos, exposed to BrdU at E9.5 (F and J), E10.5 (G and K) or E11.5 (H and L).

(I and M) Phox2a+/BrdU+ (I) or tdT+/BrdU+ (M) neurons as a percentage of all Phox2a+ or tdT+ neurons in either lamina I, lamina V/LSN, or laminae II/III (“Antenna”-like neurons) and compared between groups.

(N) Diagram of migration of spinal Phox2a neuron subpopulations.

Phox2a^{Cre}; *R26*^{LSL-tdT} embryos: (A) n = 3 E10.5, n = 3 E11.5, n = 3 E12.5, n = 3 E13.5, n = 3 E14.5, and n = 3 E15.5; (B–B’’) n = 3 E13.0 embryos; (F–M) n = 4–5 E16.5 embryos per condition. (C–E) n = 3 *TrkA*^{+/+}, n = 5 *TrkA*^{+/-}, and n = 3 *TrkA*^{-/-} E14.5 embryos.

In (D) and (E), one-way ANOVA, with Tukey’s multiple comparisons test; in (I) and (M), individual one-way ANOVAs for each neuron type with Tukey’s multiple comparisons test. **p < 0.01; ***p < 0.001. Data are represented as mean ± SEM. Scale bars: 100 μm in (A) and (C); 50 μm in (B), (C’), (F)–(H), and (J)–(L); 10 μm in (B’) and insets in (F)–(H) and (J)–(L); and 1 μm in (B’). NF-L: Neurofilament-L.

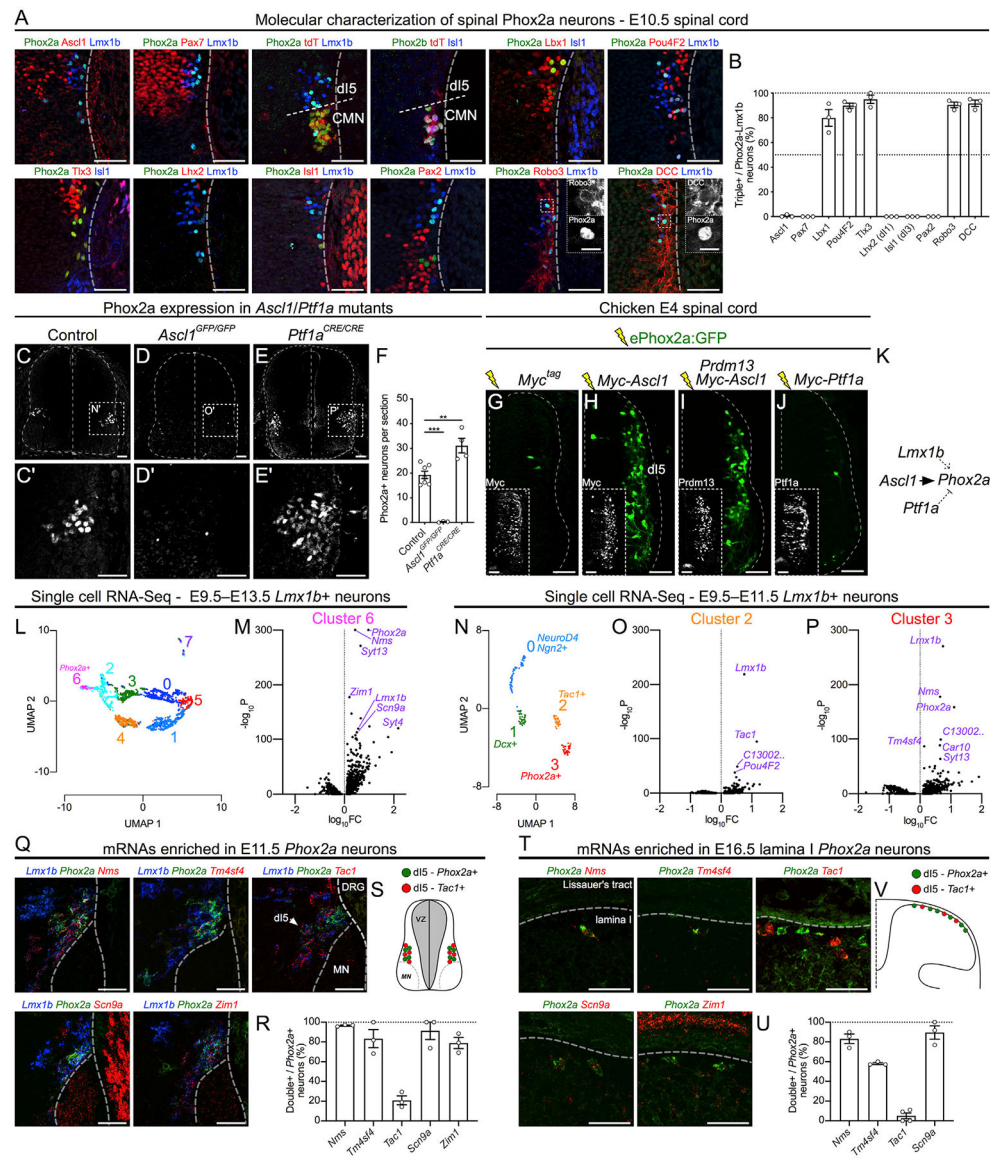


Figure 5. The Molecular Identity and Specification of Spinal Phox2a Neurons

(A) Co-expression of Phox2a with embryonic spinal neuron markers in the E10.5 *Phox2a*^{Cre}; *R26*^{LSL-tdT} spinal cord using immunohistochemistry.

(B) Quantification of each marker as a percentage of Phox2a+/Lmx1b+ neurons.

(C–F) Phox2a expression in control (C), *Ascl1* null (D), and *Ptf1a* null (E) E11.5 spinal cords, with the average number of Phox2a+ cells per section quantified in (F). (C'), (D'), and (E') show high magnification of boxed regions in (C), (D), and (E), respectively.

(G–J) Representative images from transverse sections of E4 chick neural tubes co-electroporated with the *ePhox2a-GFP* reporter and expression plasmids: control (Myc-tag only) (G), *Myc-Ascl1* (H), *Myc-Ascl1* and *Prdm13* (I), or *Myc-Ptf1a* (J). Insets show control Myc-tag, Prdm13, or Ptf1a expression.

(K) Diagram of *Phox2a* expression regulation showing direct transcriptional upregulation by *Ascl1*, upregulation by *Lmx1b* (Figure S5), and repression by *Ptf1a*. (L–P) Single-cell RNA-seq data analysis of dI5 (*Lmx1b*⁺) neurons (Delile et al., 2019).

(L and M) UMAP analysis (L) of *Lmx1b*⁺ neurons from E9.5–E13.5 compared between each other, with volcano plot of cluster-6-enriched mRNAs (M) compared to all other neurons.

(N–P) UMAP analysis (N) of *Lmx1b*⁺ neurons from E9.5–E11.5 compared between each other, with volcano plots of cluster-2-enriched mRNAs (O) and cluster-3-enriched mRNAs (P) compared to all other neurons.

(Q–V) *In situ* hybridization of select mRNAs enriched in dI5 (Q; E11.5) and lamina I neurons (T; E16.5) based on UMAP analyses. The percentage of *Phox2a*⁺ neurons co-expressing selected mRNAs are quantified at both embryonic time points in (R) and (U).

Tac1 is present in dI5 *Lmx1b*⁺ neurons and lamina I neurons that do not express *Phox2a*, as depicted in diagrams in (S) and (V).

Phox2a^{Cre}; *R26*^{LSL-tdT+} embryos: (A and B) n = 3 E10.5; (Q and R) n = 3 E11.5; (T and U) n = 3–4 E16.5 embryos. (C–F) n = 6 control, n = 3 *Ascl1*^{GFP/GFP}, and n = 4 *Ptf1a*^{Cre/Cre} embryos. (G–J) n = 6 E4 chicken embryos for each condition. Student's t test in (F); **p < 0.01; ***p < 0.001. Data are represented as mean ± SEM. Data in (L)–(P) are derived from Delile et al. (2019); data processing and statistics are described in STAR Methods. Scale bars: 50 μm for all, except 10 μm for insets in (A). DRG, dorsal root ganglion; FC, fold change; MN, motor neuron.

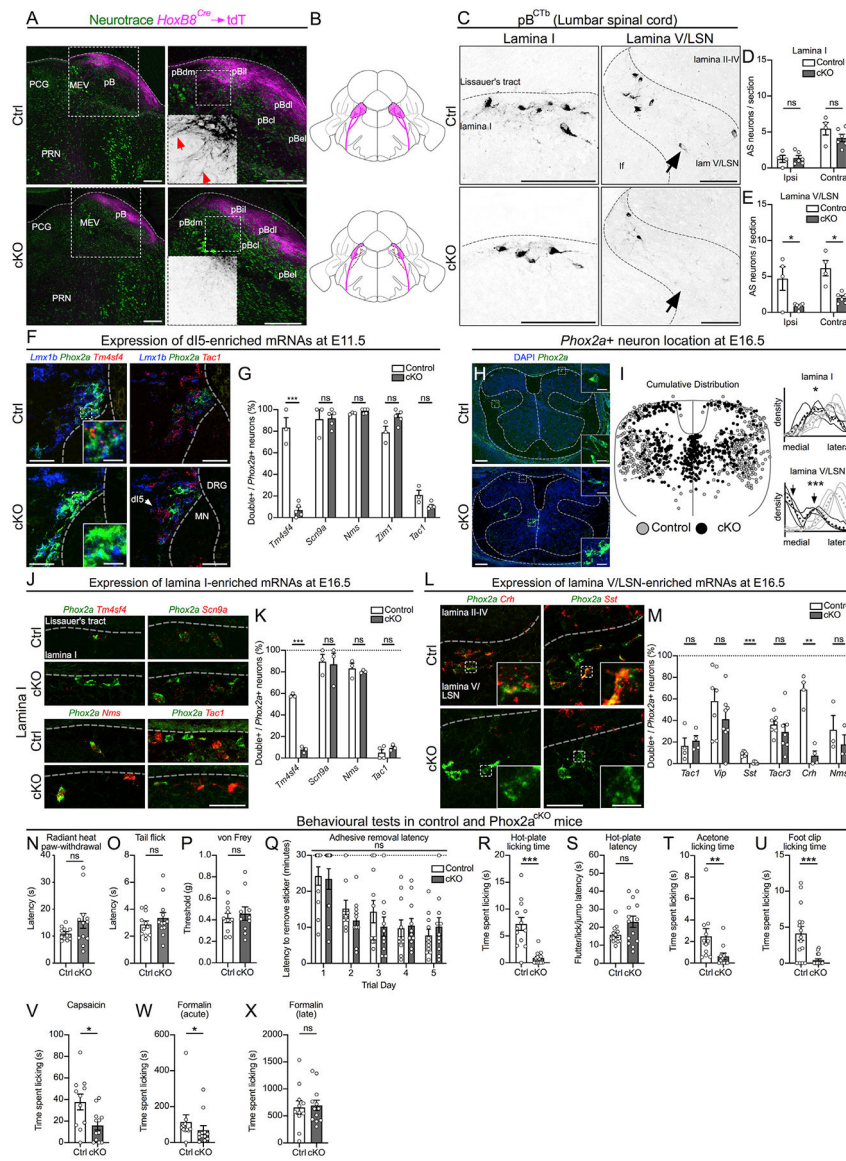


Figure 6. *Phox2a* Is Required for the Normal Development and Function of a Subset of AS Neurons

(A) The parabrachial nucleus (pB) of control (*Hoxb8^{Cre}; Phox2a^{+/+}; R26^{LSL-tdT}⁺*; Ctrl, top row) and *Phox2a^{cKO}* (*Hoxb8^{Cre}; Phox2a^{fl/fl}; R26^{LSL-tdT}⁺*; cKO, bottom row) adult mice, depicting spinoparabrachial axons labeled via *Hoxb8^{Cre}*-driven axonal tdT expression. Right panels show magnified views of the left panels, with insets depicting tdT axons (red arrows). (B) Diagram depicting the loss of spinal afferents (magenta) to the pB of *Phox2a^{cKO}* mice. (C–E) Spinal neurons labeled by CTb injections in the pB, in lamina I (left column of C, quantified in D) and lamina V/LSN (right column of C, quantified in E), in control (top row) and *Phox2a^{cKO}* (bottom row) adult mice. (F and G) Co-expression of *Phox2a* and *Lmx1b* with dl5-enriched mRNAs in control (top row) and *Phox2a^{cKO}* (bottom row) E11.5 spinal cords (F), quantified as a percentage of *Phox2a⁺* neurons (G). See Figure S6 for additional images. (H and I) Distribution of *Phox2a⁺* neurons in E16.5 control and *Phox2a^{cKO}* mouse embryos.

(H) Insets show individual *Phox2a*⁺ cells magnified.

(I) Individual *Phox2a* neuron locations (left) and density plots of *Phox2a*⁺ neurons (right) derived from 3–5 sections (10 μ m) of 4 control (gray) and 4 *Phox2a*^{cKO} (black) E16.5 spinal cords. Coordinates and mediolateral distribution are normalized to the width and height of an idealized spinal cord. Individual lines on density plots represent single animals, dotted lines represent mean distribution of 4 animals, gray lines represent control embryos, and black lines represent *Phox2a*^{cKO} *Phox2a*⁺ cells. Black arrows point to the bimodal distribution of *Phox2a*^{cKO} *Phox2a*⁺ cells in deep laminae. Average mediolateral positions of lamina I and lamina V/LSN neurons are statistically compared.

(J and K) Co-expression of *Phox2a* with dI5-enriched mRNAs in lamina I of control (top row) and *Phox2a*^{cKO} (bottom row) E16.5 spinal cords (J), quantified as a percentage of *Phox2a*⁺ neurons (K).

(L and M) Co-expression of *Phox2a* and candidate lamina V/LSN neuron marker mRNAs in lamina V/LSN neurons of control (top row) and *Phox2a*^{cKO} (bottom row) E16.5 spinal cords (L), quantified as a percentage of *Phox2a*⁺ neurons (M). See Figure S6 for additional images.

(N–X) Behavioral tests in control and *Phox2a*^{cKO} mice. (N) Radiant heat paw-withdrawal assay; n = 11 control, and n = 12 *Phox2a*^{cKO}. (O) Hot-water tail flick assay; n = 11 control, and n = 12 *Phox2a*^{cKO}. (P) von Frey test; n = 10 control, and n = 10 *Phox2a*^{cKO}. (Q) Adhesive removal latency; n = 11 control, and n = 10 *Phox2a*^{cKO}. (R and S) Time spent licking (R) and latency to any response (S) during the hot-plate test; n = 13 control, and n = 14 *Phox2a*^{cKO}. (T) Acetone test; n = 11 control, and n = 11 *Phox2a*^{cKO}. (U) Foot clip test; n = 15 control, and n = 16 *Phox2a*^{cKO}. (V) Capsaicin test; n = 11 control, and n = 12 *Phox2a*^{cKO}. (W and X) Formalin test (acute phase in W; late phase in X); n = 11 control, and n = 12 *Phox2a*^{cKO}.

In (A), n = 4 control, and n = 4 *Phox2a*^{cKO} adult mice. (C–E) n = 4 control, and n = 6 *Phox2a*^{cKO} adult mice. (F and G) n = 3 control, and n = 5 *Phox2a*^{cKO} E11.5 mice. (H and I) n = 4 control, and n = 4 *Phox2a*^{cKO} E16.5 mice. (J and K) n = 3–4 control, and n = 3 *Phox2a*^{cKO} E16.5 mice. (L and M) n = 3–8 control, and n = 3–8 *Phox2a*^{cKO} E16.5 mice. (N–X) The ns are given above.

In (D) and (E), two-way ANOVA with Tukey's multiple comparisons test; in (I), unpaired t test; in (G), (K), and (M), multiple t tests using the Holm-Sidak method; in (Q), mixed-effects analysis with Sidak's multiple comparisons test; and Mann-Whitney test in (N)–(P) and (R)–(X). ns, non-significant; *p < 0.05; **p < 0.01; ***p < 0.001. Data are represented as mean \pm SEM. Scale bars: 250 μ m in (A); 50 μ m in (C); (H) 100 μ m in (H); 20 μ m in insets for (H); 50 μ m in (F), (J), and (L); and 10 μ m in insets for (F), (J), and (L). Images in Figure 5Q have been re-used in Figure 6F, and images in Figure 5T have been re-used in Figure 6J. Data from Figures 5R and 5U representing the above images are re-used in Figures 6G and 6K, respectively. These data were collected and analyzed as a single experiment.

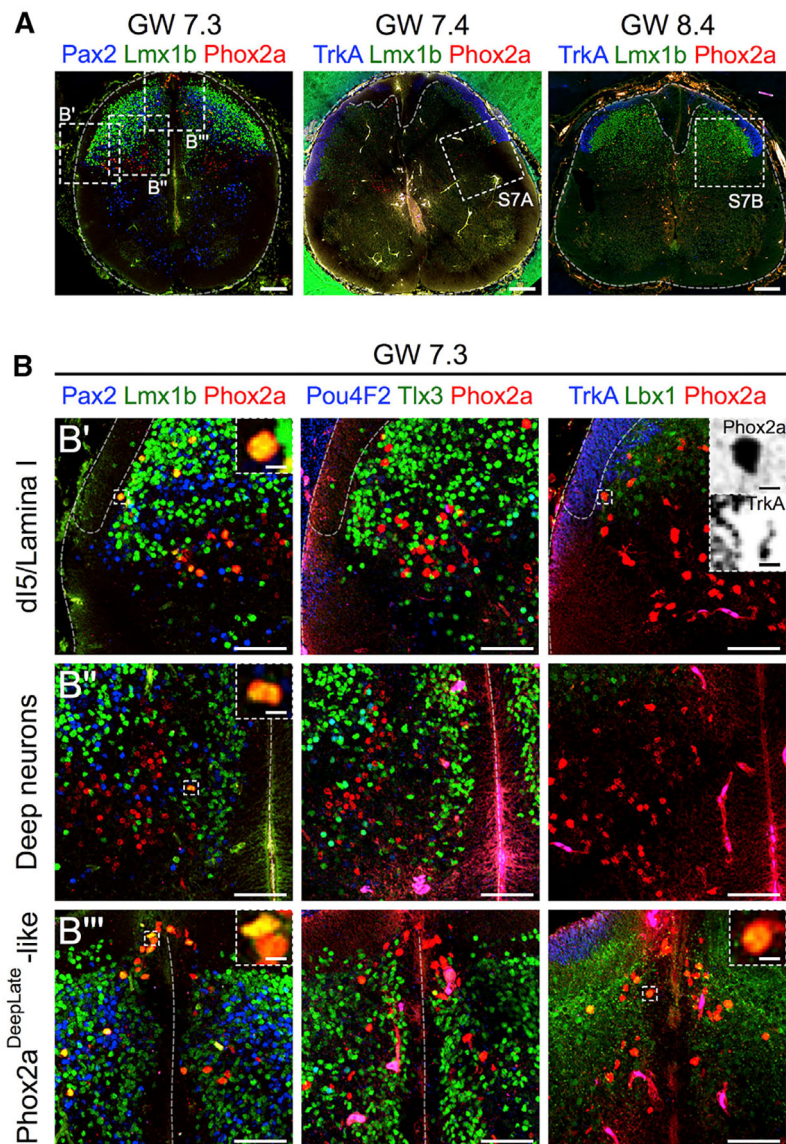


Figure 7. Phox2a Neuron Molecular Identity Is Conserved in the Developing Human Spinal Cord

(A) Sections of GW7.3–GW8.4 human spinal cords showing Phox2a, Lmx1b, TrkA, and Pax2 expression. Location of higher magnification panels is shown in boxed regions. (B–B''') In (B): Phox2a, Lmx1b, Pax2, Pou4F2, Tlx3, Lbx1, and TrkA expression in the GW7.3 spinal cord, demonstrating co-labeling of Phox2a neurons with dorsal horn markers Lmx1b and Lbx1, but not with Pax2, Pou4F2, or Tlx3, in a Phox2a^{LamI}/Phox2a^{DeepEarly}-like cluster (B'), the deep dorsal horn (B''), and a Phox2a^{DeepLate}-like cluster near the roof plate (B'''). Top right panel shows apposition of Phox2a cells with TrkA+ sensory afferents, similar to that in mouse (Figure 4). Insets show higher magnification of boxed regions (TrkA and Phox2a channels split and inverted).

In (A), three human embryonic spinal cords (GW7.3, GW7.4, and GW8.4) are represented. In (B), one GW7.3 human embryonic spinal cord from (A) is represented. Scale bars: 200 μm in (A), 100 μm in (B), and 10 μm in insets in (B')–(B''')

KEY RESOURCES TABLE

REAGENT or RESOURCE	SOURCE	IDENTIFIER
Antibodies		
Rabbit anti-Phox2a (1:10,000 from frozen stock; Figures 1, 2, 3, 4, 5, and 6)	Jean-François Brunet (École normale supérieure, Paris, France)	(Tiveron et al., 1996) RRID: AB_2315159
Rabbit anti-Phox2a (Figure 7; and 1:1000 for mouse, 1:500 for human embryo)	Abcam	Cat#: Ab155084 Lot#: GR117345–3 RRID: N/A
Rabbit anti-Phox2b (1:10,000 from frozen stock)	Jean-François Brunet (École normale supérieure, Paris, France)	(Pattyn et al., 1997) RRID: AB_2315160
Rabbit anti-RFP (red fluorescent protein) (1:1000)	Rockland	Cat#: 600-401-379 RRID: AB_2209751
Mouse anti-NeuN (1:1000)	Millipore	Cat#: MAB377 RRID: AB_2298772
Guinea Pig anti-vGlut2 (1:1000)	Synaptic Systems	Cat#: 135–404 RRID: AB_887884
Rat anti-Bromodeoxyuridine (BrdU) (1:10,000)	Abcam	Cat# ab6326: RRID: AB_305426
Goat anti-rTrkA (1:1000 for mouse, 1:500 for human embryo)	R&D Systems	Cat#: Af1056 RRID: AB_2283049
Mouse anti-Islet1 (1:100)	Developmental Studies Hybridoma Bank (DSHB)	Cat#: 39.3F7 RRID: AB_1157901
Mouse anti-Pax7 (1:100)	DSHB	Cat#: pax7 RRID: AB_528428
Mouse anti-Lhx2 (1:100)	DSHB	Cat#: Lhx2–1C11 RRID: AB_2618817
Mouse anti-Nkx6.1 (1:100)	DSHB	Cat#: F55A10 RRID: AB_532378
Mouse anti-Neurofilament-L (NF-L)	DSHB	Cat#: 2H3 RRID: AB_531793
Goat anti-hPax2 (1:1000 for mouse, 1:500 for human embryo)	R&D Systems	Cat#: AF3364 RRID: AB_10889828
Guinea Pig anti-Lbx1 (1:10000 for mouse, 1:5000 for human embryo)	Carmen Birchmeier (Max Delbrück Center, Berlin, Germany)	RRID: AB_2532144
Guinea Pig anti-Lmx1b (1:10000 for mouse, 1:5000 for human embryo)	Carmen Birchmeier (Max Delbrück Center, Berlin, Germany)	RRID: AB_2314752
Guinea Pig anti-Tlx3 (1:10000 in mouse, 1:10000 for chick, 1:5000 for human embryo)	Carmen Birchmeier (Max Delbrück Center, Berlin, Germany)	RRID: AB_2532145
Guinea pig anti-PRDM13 (1:1000)	Takahisa Furukawa (Osaka University, Osaka, Japan)	(Watanabe et al., 2015) RRID: N/A
Guinea pig anti-PTF1A (1:10000)	Jane Johnson (University of Texas Southwestern, Dallas, United States)	TX507 RRID: N/A
Mouse anti-MYC (1:1000)	Abcam	Cat# ab32 RRID: AB_303599
Goat anti-Brn3b (Pou4F2), (1:1000 for mouse, 1:500 for human embryo)	Santa Cruz Biotechnology	Cat#: sc-6026 RRID: AB_673441
Mouse anti-Ascl1 (1:100)	Santa Cruz Biotechnology	Cat#: sc-390794 RRID: N/A
Mouse anti-Ascl1 (1:100)	Santa Cruz Biotechnology	Cat#: sc-374550 RRID: AB_10985986
Mouse anti-Ascl1 (1:100)	Santa Cruz Biotechnology	Cat# sc-374104 RRID: AB_10918561
Goat anti-hRobo3	R&D Systems	Cat# AF3076 RRID: AB_2181865
Goat anti-mDcc	R&D Systems	Cat# AF844 RRID: AB_2089765

REAGENT or RESOURCE	SOURCE	IDENTIFIER
Rat anti-Pou6F2 (1:2000)	Jay Bikoff (Thomas Jessell Laboratory, HHMI Columbia University, New York, United States)	Cat# CU1796 RRID: AB_2665427
Rabbit anti-Shox2 (1:200)	Laskaro Zagoraiou (Thomas Jessell Laboratory, HHMI Columbia University, New York, United States)	(Dougherty et al., 2013) RRID: N/A
Sheep anti-FoxP2 (1:2000)	R&D Systems	Cat#: AF5647 RRID: AB_2107133
Alexa 488 Donkey anti-Rabbit (1:500)	Jackson Immunoresearch Laboratories	Cat#: 711-545-152 Lot#: 141848 RRID: AB_2313584
Alexa 488 Donkey anti-Guinea Pig (1:500)	Jackson Immunoresearch Laboratories	Cat#: 706-545-148 Lot#: 138058 RRID: AB_2340472
Alexa 488 Donkey anti-Mouse (1:500)	Jackson Immunoresearch Laboratories	Cat#: 715-545-150 Lot#: 136831 RRID: AB_2340846
Alexa 488 Donkey anti-Goat (1:500)	Jackson Immunoresearch Laboratories	Cat#: 705-545-147 Lot#: 136089 RRID: AB_2336933
Alexa 488 Donkey anti-Rat (1:500)	Jackson Immunoresearch Laboratories	Cat#: 712-545-153 Lot#: 138117 RRID: AB_2340684
Alexa 488 Donkey anti-Sheep (1:500)	Jackson Immunoresearch Laboratories	Cat#: 713-545-003 Lot#: N/A RRID: AB_2340744
Cy3 Donkey anti-Rat (1:500)	Jackson Immunoresearch Laboratories	Cat#: 712-165-153 Lot#: 139289 RRID: AB_2340667
Cy3 Donkey anti-Rabbit (1:500)	Jackson Immunoresearch Laboratories	Cat#: 711-165-152 Lot#: 138270 RRID: AB_2307443
Cy3 Donkey anti-Mouse (1:500)	Jackson Immunoresearch Laboratories	Cat#: 715-165-150 Lot#: N/A RRID: AB_2340813
Cy3 Donkey anti-Goat (1:500)	Jackson Immunoresearch Laboratories	Cat#: 705-165-147 Lot#: 134527 RRID: AB_2307351
Cy5 Donkey anti-Rabbit (1:500)	Jackson Immunoresearch Laboratories	Cat#: 711-175-152 Lot#: 138336 RRID: AB_2340607
Cy5 Donkey anti-Mouse (1:500)	Jackson Immunoresearch Laboratories	Cat#: 715-175-150 Lot#: 135323 RRID: AB_2340819
Cy5 Donkey anti-Goat (1:500)	Jackson Immunoresearch Laboratories	Cat#: 705-175-147 Lot#: 134531 RRID: AB_2340415
Cy5 Donkey anti-Guinea Pig (1:500)	Jackson Immunoresearch Laboratories	Cat#: 706-175-148 Lot#: 136607 RRID: AB_2340462
Chemicals, Peptides, and Recombinant Proteins		
NeuroTrace 435/455 Blue Fluorescent Nissl Stain	ThermoFisher Scientific	Cat#: N21479 RRID: N/A
NeuroTrace 500/525 Green Fluorescent Nissl Stain	ThermoFisher Scientific	Cat#: N21480 RRID: N/A
2-Hydroxystilbene-4,4'-dicarboximidine (fluorogold)	ThermoFisher Scientific	Cat#: H22845 RRID: N/A
Alexa 488-conjugated Cholera toxin B	ThermoFisher Scientific	Cat#: C22841 Lot#: 2038245 RRID: N/A
5-bromo-2'-deoxyuridine (BrdU)	ThermoFisher Scientific	Cat#: B23151 Lot#: 1916418 RRID: N/A
Paraformaldehyde	Millipore Sigma	Cat#: P6148 RRID: N/A
(E)-Capsaicin	Tocris	Cat#: 0462 Lot#: 7A/218361 RRID: N/A
4',6-diamidino-2-phenylindole (DAPI)	Thermo Fisher Scientific	Cat# D1306
Mowiol (Polyvinyl alcohol)	Millipore Sigma	Cat#: 81381 RRID: N/A
Experimental Models: Organisms/Strains		
Mice - Phox2a ^{Cre}	This manuscript	RRID: N/A

REAGENT or RESOURCE	SOURCE	IDENTIFIER
Mice - HoxB8 ^{Cre} (Tg(Hoxb8-cre)1403Uze)	Hanns Ulrich Zeilhofer, ETH Zürich, Zurich, Switzerland)	Cat#: MGI: 4881836 RRID: N/A
Mice - Cdx2 ^{FlpO} (Tg(CDX2-flpo)#Gld)	Martyn Goulding (Salk Institute, San Diego, United States)	Cat#: MGI: 5911680 RRID: N/A
Mice - Ai14 (B6;129S6-Gt(ROSA)26Sortm14(CAG-tdTomato)Hze/J)	The Jackson Laboratory	Cat#: JAX:007908 RRID: IMSR_JAX:007908
Mice - Ai65 (B6;129S-Gt(ROSA)26Sortm65.1(CAG-tdTomato)Hze/J)	The Jackson Laboratory	Cat#: JAX:021875 RRID: IMSR_JAX:021875
Mice - Phox2alox (B6D2.129S2-Phox2atm2Jbr/Orl)	European Mutant Mouse Archive (EMMA)	Cat#: EM:04758 RRID:IMSR_EM:04758
Mice - TrkA ^{-/-} (Ntrk1 ^{tm1Par})	Lino Tessarollo (National Cancer Institute, Frederick, MD, United States)	(Liebl et al., 2000) Cat#: MGI: 1933963 RRID: N/A
Mice - <i>Ptf1atm1</i> (cre)Wri	Christopher Wright (Vanderbilt University, Nashville, United States)	(Kawaguchi et al., 2002) Cat#: MGI: 2387812 RRID: N/A
Mice - <i>Asc11tm1Reed/J</i>	The Jackson Laboratory	Cat# JAX:012881 RRID: IMSR_JAX:012881
Mice - C57BL/6J	The Jackson Laboratory	Cat# JAX:000664 RRID: IMSR_JAX:000664
Mice - 129S1/SvImJ	The Jackson Laboratory	Cat# JAX:002448 RRID: IMSR_JAX:002448
Mice - B6C3F1/J	The Jackson Laboratory	Cat# JAX: 100010 RRID: IMSR_JAX: 100010
Oligonucleotides		
RNA Scope Probe - Mm-Tac1 C1	Advanced Cell Diagnostics	Cat#: 410351 Lot#: 18354A RRID: N/A
RNA Scope Probe - Mm-Phox2a C2	Advanced Cell Diagnostics	Cat#: 520371-C2 Lot#: N/A RRID: N/A
RNA Scope Probe - Mm-Lmx1b C3	Advanced Cell Diagnostics	Cat#: 412931-C3 Lot#: N/A RRID: N/A
RNA Scope Probe - Mm-Nms C1	Advanced Cell Diagnostics	Cat#: 472331 Lot#: TBD RRID: N/A
RNA Scope Probe - Mm-Tm4sf4 C1	Advanced Cell Diagnostics	Cat#: 819831 Lot#: N/A RRID: N/A
RNA Scope Probe - Mm-Zim1 C1	Advanced Cell Diagnostics	Cat#: 819821 Lot#: N/A RRID: N/A
RNA Scope Probe - Mm-Scn9a C1	Advanced Cell Diagnostics	Cat#: 313341 Lot#: N/A RRID: N/A
RNA Scope Probe - Mm-Pdzrn3 C1	Advanced Cell Diagnostics	Cat#: 517061 Lot#: 17269A RRID: N/A
RNA Scope Probe - Mm-Syt4 C1	Advanced Cell Diagnostics	Cat#: 574731 Lot#: N/A RRID: N/A
RNA Scope Probe - Mm-VIP C1 (Vasoactive Intestinal Polypeptide)	Advanced Cell Diagnostics	Cat#: 415961 Lot#: 19045A RRID: N/A
RNA Scope Probe - Mm-Sst C1	Advanced Cell Diagnostics	Cat#: 404631 Lot#: N/A RRID: N/A
RNA Scope Probe - Mm-TacR3 C1	Advanced Cell Diagnostics	Cat#: 481671 Lot#: 18254A RRID: N/A
RNA Scope Probe - Mm-Crh C1	Advanced Cell Diagnostics	Cat#: 316091 Lot#: N/A RRID: N/A
RNA Scope Probe - Mm-Slc17A6 C1 (vGlut2)	Advanced Cell Diagnostics	Cat#: 319171 Lot#: 19052B RRID: N/A
RNA Scope Probe - Mm-Slc32A1 C1 (vGAT)	Advanced Cell Diagnostics	Cat#: 319191 Lot#: 19057A RRID: N/A
RNA Scope Probe - Mm-TacR1 C1	Advanced Cell Diagnostics	Cat#: 428781 Lot#: 19057A RRID: N/A
RNA Scope Probe - Mm-Cck C1 (Cholecystokinin)	Advanced Cell Diagnostics	Cat#: 402271 Lot#: 19057A RRID: N/A
RNA Scope Probe - Mm-Lypd1 C1	Advanced Cell Diagnostics	Cat#: 318361 Lot#: 18353B RRID: N/A
RNA Scope Probe - Mm-Gal C1 (Galanin)	Advanced Cell Diagnostics	Cat#: 400961 Lot#: 18277C RRID: N/A

REAGENT or RESOURCE	SOURCE	IDENTIFIER
RNA Scope Probe - Mm-pDyn C1 (preproDynorphin)	Advanced Cell Diagnostics	Cat#: 318771 Lot#: 18303A RRID: N/A
RNA Scope Probe - Mm-pNoc C1 (prepronociceptin)	Advanced Cell Diagnostics	Cat#: 437881 Lot#: 19016B RRID: N/A
Genotyping primers		
Cre-1: 5'-AGG TGT AGA GAA GGC ACT TAG C-3' Expected band size: 412 bp (only one band)	This manuscript	N/A
Cre-2: 5'-CTA ATC GCC ATC TTC CAG CAG G-3'	This manuscript	N/A
FLPo-1: 5'-TGA GCT TCG ACA TCG TGA AC-3' Expected band size: 350 bp (only one band)	Martyn Goulding (Salk Institute, San Diego, United States)	N/A
FLPo-2: 5'-ACA GGG TCT TGG TCT TGG TG-3'	Martyn Goulding (Salk Institute, San Diego, United States)	N/A
Ai14-1: 5'-TCA ATG GGC GGG GGT CGT T-3' Expected band sizes: WT: 350 bp, Mutant: 250 bp	This manuscript	N/A
Ai14-2: 5'-CTC TGC TGC CTC CTG GCT TCT-3'	This manuscript	N/A
Ai14-3: 5'-CGA GGC GGA TCA CAA GCA ATA-3'	This manuscript	N/A
Ai65 WT1: "oIMR9020" 5'-AAG GGA GCT GCA GTG GAG TA-3' Expected band size: 315 bp	The Jackson Laboratory	N/A
Ai65 WT2: "oIMR9021" 5'-CCG AAA ATC TGT GGG AAG TC-3'	The Jackson Laboratory	N/A
Ai65 Mutant1: "oIMR9103" 5'-GGC ATT AAA GCA GCG TAT CC-3' Expected band size: 297 bp	The Jackson Laboratory	N/A
Ai65 Mutant2: "oIMR9105" 5'-CTG TTC CTG TAC GGC ATG G-3'	The Jackson Laboratory	N/A
Phox2a ^{fl} -1: 5'-GCC TCC AAC TCC ATA TTC C-3' Expected band sizes: WT: 150bp, Flox: 200bp	Jean-François Brunet (École normale supérieure, Paris, France)	N/A
Phox2a ^{fl} -2: 5'-ATC AGG AGT CAG TCG TCT G-3'	Jean-François Brunet (École normale supérieure, Paris, France)	N/A
TrkA-WT-5': 5'-TGT ACG GCC ATA GAT AAG CAT-3' Expected WT band size: 160 bp	Lino Tessarollo (National Cancer Institute, Frederick, MD, United States)	N/A
TrkA-WT-3': 5'-TTG CAT AAC TGT GTA TTT CAC-3'	Lino Tessarollo (National Cancer Institute, Frederick, MD, United States)	N/A
TrkA-mutant (pGKneopolyA) forward primer: 5'-CGC CTT CTT GAC GAG TTC TTC TG-3' Expected mutant band size: 550 bp	Lino Tessarollo (National Cancer Institute, Frederick, MD, United States)	N/A
Recombinant DNA		
Plasmid: pMiWIII-Myc- ASCL1	Jane Johnson (University of Texas Southwestern, Dallas, United States)	N/A
Plasmid: pMiWIII-Myc- PTF1A	Jane Johnson (University of Texas Southwestern, Dallas, United States)	N/A
Plasmid: pMiWIII-Prdm13	Jane Johnson (University of Texas Southwestern, Dallas, United States)	N/A
Plasmid: pMiWIII-Myc-tag	Jane Johnson (University of Texas Southwestern, Dallas, United States)	N/A

REAGENT or RESOURCE	SOURCE	IDENTIFIER
Plasmid: pMCSIII-ePhox2a	This manuscript	N/A
Software and Algorithms		
Graphpad Prism 8 (macOS) - Version 8.3.0	Graphpad Software	https://www.graphpad.com/scientific-software/prism RRID: SCR_002798
Bioseb T2CT - Version 2.2.4	Bioseb	https://www.bioseb.com/en/pain-thermal-allodynia-hyperalgesia/897-thermal-place-preference-2-temperatures-choice-nociception-test.html RRID: N/A
ImageJ - Version 2.0.0	National Institutes of Health	https://imagej.nih.gov/ij/ RRID: SCR_003070
Photoshop and Illustrator	Adobe	N/A
Excel for Mac 2011 v14.7.7	Microsoft	N/A
Aegisub v3.2.2	Aegisub	http://www.aegisub.org/
Other		
Stereotaxic frame and digital display	David Kopf Instruments	Cat#: 940, 960, 1770, 900C, 922, 933-B RRID: N/A
Stereotaxic syringe pump with Micro4 controller	David Kopf Instruments	Cat#: UMP3-1, 1770-C RRID: N/A
Touch Test Sensory Evaluators (0.008, 0.02, 0.04, 0.07, 0.16, 0.4, 0.6, 1, 1.4, 2g)	North Coast Medical	Cat#: NC12775-01 - NC12775-10 RRID: N/A
IITC Hot Cold-Plate Analgesia Meter for Mice and Rats	IITC	Cat#: PE34 RRID: N/A
Thermal Place Preference, 2 Temperatures Choice Nociception Test	Bioseb	Cat#: BIO-T2CT RRID: N/A
iPhone SE-Version 12.3.1	Apple	Cat#: iPhone SE. RRID: N/A
Micro Toothless Alligator Test Clip (Copper Plated)	https://www.amazon.com/Toothless-Alligator-Copper-Plated-Microscopic/dp/B0187MIUU4	Cat#: CECOMINOD005515 RRID: N/A
Confocal Microscope	Zeiss	Cat#: LSM-710
Confocal Microscope	Leica	Cat#: SP8
Epifluorescence Upright Microscope	Leica	Cat#: DM6000
Epifluorescence Upright Microscope	Leica	Cat#: DM6
Epifluorescence Dissecting Stereomicroscope	Leica	Cat#: MZ16FA